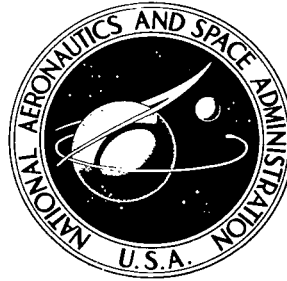


NASA TECHNICAL NOTE



NASA TN D-5337

c. 1

NASA TN D-5337



LOAN COPY: RETURN --
AFWL (WL0L)
KIRTLAND AFB, N MEX

INTERCOMPARISON OF THE MINITRACK AND OPTICAL TRACKING NETWORKS USING GEOS I LONG-ARC ORBITAL SOLUTIONS

by

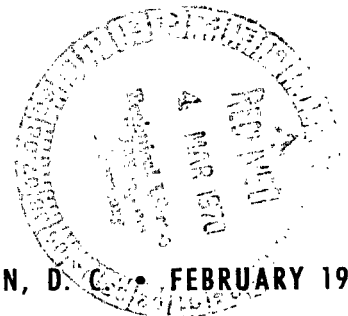
James G. Marsh and Clarence E. Doll, Jr.

Goddard Space Flight Center

and

Richard J. Sandifer and Wayne A. Taylor

Wolf Research and Development Corporation



NATIONAL AERONAUTICS AND SPACE ADMINISTRATION • WASHINGTON, D. C. • FEBRUARY 1970



INTERCOMPARISON OF THE MINITRACK
AND OPTICAL TRACKING NETWORKS USING
GEOS I LONG-ARC ORBITAL SOLUTIONS

By James G. Marsh and Clarence E. Doll, Jr.

Goddard Space Flight Center
Greenbelt, Md.

and

Richard J. Sandifer and Wayne A. Taylor
Wolf Research and Development Corporation
Bladensburg, Md.

NATIONAL AERONAUTICS AND SPACE ADMINISTRATION

For sale by the Clearinghouse for Federal Scientific and Technical Information
Springfield, Virginia 22151 - CFSTI price \$3.00

ABSTRACT

STADAN Minitrack network data can be adequately analyzed using an optically determined "standard orbit" of 5-1/4 days based primarily upon GEOS I flashing-lamp sequence observations recorded by STADAN and SPEOPT cameras. A technique has been devised to uncouple the refraction-dependent from the refraction-independent effects in the Minitrack residuals. Results indicate the Minitrack system as a whole to be free of any strong bias. Station-dependent systematic errors were not removed by the usual calibration procedures, and accordingly an optically-determined "standard orbit" would be a preferable method of calibrating individual Minitrack antenna arrays. A Minitrack orbit for the same time period as the optical orbit was obtained, and position differences between the two orbits produced an rms deviation of approximately 165 meters—a favorably small figure.

SUMMARY

STADAN Minitrack network data are analyzed using an optically determined "standard orbit" 5-1/4 days in length as a reference orbit. This "standard orbit" has an rms fit of 3'0. It is shown that this is adequate for evaluating Minitrack data. The "standard orbit" is based primarily upon GEOS I flashing-lamp sequence observations recorded by STADAN and SPEOPT MOTS 24" and 40", SAO Baker-Nunn, and USAF PC-1000 cameras.

A technique is devised to uncouple the refraction-dependent from the refraction-independent effects in the Minitrack residuals. The mean value of the refraction-dependent residuals exhibited a shift of -0.2×10^{-3} in the region of 10° to 30° elevation. The shift is insignificant at higher elevations. The mean value of the refraction-independent residuals is approximately 0.02×10^{-3} with a standard deviation of 0.2×10^{-3} . This small mean value indicates that the Minitrack system when viewed as a whole appears relatively free of any strong bias. The Minitrack data were not included in the reference orbital solution. Analysis of the residuals by individual stations indicates that there may be some station-dependent systematic errors present. Since these systematic errors were not removed by the usual calibration procedures, it is suggested that the use of an optically-determined "standard orbit" would be a preferable method of calibrating individual Minitrack antenna arrays.

A Minitrack orbit for the same time period as the optical orbit was obtained with an rms fit of 0.19×10^{-3} . The Minitrack data used in this particular solution were not corrected for ionospheric or tropospheric refraction and were not weighted for elevation effects. Data down to 15° elevation were used in the solution. Position differences between the Minitrack and optical orbits produced an rms deviation of approximately 165 meters. This low figure is due in part to the use of an accurate gravity model and of station positions consistent with this gravity model.

ABBREVIATIONS USED IN THIS DOCUMENT

MOTS	Minitrack Optical Tracking System
SAO	Smithsonian Astrophysical Observatory
SPEOPT	Special Optical Tracking System (Same cameras used by MOTS)
STADAN	Satellite Tracking and Data Acquisition Network

TRACKING-STATION CODE NAMES

A detailed description of the names, general locations, and specific coordinates of the tracking stations corresponding to the adopted six-character station code names used in the various tables and figures of this document is given in Appendix D.

CONTENTS

Abstract	ii
Summary	iii
Abbreviations; Tracking-Station Code Names	iv
INTRODUCTION	1
FEASIBILITY OF USING OPTICALLY-DETERMINED "STANDARD ORBITS" TO EVALUATE AND CALIBRATE MINITRACK DATA	2
SUMMARY OF OPTICAL DATA USED IN THE "STANDARD ORBIT" SOLUTION	3
SUMMARY OF MINITRACK DATA AVAILABLE FROM THE SPACE SCIENCE DATA CENTER FOR THE PERIOD OF INTEREST, AND DATA REJECTED BEFORE ANALYSIS	7
GEOMETRY OF THE MINITRACK "EQUATORIAL" AND "POLAR" MODES OF TRACKING	11
USE OF THE MINITRACK GEOMETRY TO UNCOUPLE REFRACTION- DEPENDENT FROM REFRACTION-INDEPENDENT EFFECTS IN THE MINITRACK RESIDUALS	13
CONSIDERATION OF RESIDUALS FROM THE MINITRACK NETWORK AS A WHOLE	13
SYSTEMATIC ERRORS AT INDIVIDUAL MINITRACK SITES	15
DIFFERENCES IN ORBITS ADJUSTED USING MINITRACK DATA ONLY AND OPTICAL DATA ONLY	24
CONCLUSIONS	25
References	26
Bibliography	27
Appendix A—Brief Description of the 136-Mc Minitrack Interferometer Tracking System	29
Appendix B—Preprocessing of Optical Observations	35
Appendix C—Force Models Used in NONAME	39
Appendix D—Tracking Station Coordinates	45
Appendix E—Table of GEOS I Orbit Numbers from 12/31/65 to 1/5/66	59

INTERCOMPARISON OF THE MINITRACK AND OPTICAL TRACKING NETWORKS USING GEOS I LONG-ARC ORBITAL SOLUTIONS

by

James G. Marsh and Clarence E. Doll, Jr.
Goddard Space Flight Center

and

Richard J. Sandifer and Wayne A. Taylor
Wolf Research and Development Corporation

INTRODUCTION

The primary objectives of the GEOS I project are to use observations of GEOS I for the purposes of connecting geodetic datums and defining the earth's gravitational field to a specified degree of accuracy, improving positional accuracies of satellite tracking sites, and evaluation and calibration of tracking equipment (Reference 1, pp. 1, 6). This report is concerned with the last-named aspect of evaluation and calibration as applied to the Minitrack system.

One particular phase of the Minitrack/optical data intercomparison is presented in this report. GEOS I long-arc orbital solutions determined by optical observations only are used as a "standard orbit." The Minitrack residuals used in this analysis are calculated on the basis of this optically-determined "standard orbit." As a result, the Minitrack residuals are calculated on the basis of an adjusted orbit which is not influenced by the Minitrack data set itself. Assuming that there are no significant systematic differences between the two data types, or—perhaps equally important—no significant systematic differences between the tracking networks which recorded the two data types, this type of intercomparison can provide a useful tool for analyzing and evaluating the Minitrack data and network. It will be shown in a later section that the geometry of the reception pattern of the Minitrack antenna arrays provides a possible method of uncoupling refraction-dependent effects from refraction-independent effects contained in the Minitrack residuals. In order to analyze the data from this viewpoint, the Minitrack residuals have been calculated from data which have not been preprocessed. As a result, the full effects of both tropospheric and ionospheric refraction are included in the residuals. By analyzing the data in this manner, it may be possible to determine how successfully the uncoupling process can be performed. If the process is successful, there is the added advantage that the data do not contain erroneous refraction effects which may arise from over-correcting or under-correcting the data for refraction. This problem is particularly sensitive because of the large uncertainties contained in present knowledge of the state of the ionosphere. The analysis in this report will be restricted to Minitrack data with all refraction effects included.

The last section herein before "conclusions" presents an intercomparison of two 5-1/4-day trajectories. One trajectory was computed on the basis of initial conditions adjusted by optical data only. The second trajectory was computed on the basis of initial conditions adjusted by Minitrack data only.

Using the optically-determined orbit as the standard, the errors in position as determined by the Minitrack data had a standard deviation of approximately 165 meters. The Minitrack solution utilized data down to approximately 15° elevation. These data were not corrected for tropospheric or ionospheric refraction, and were not weighted to compensate for any deterioration of the data at the lower elevations. The reduction of the standard deviation to the relatively low value of 165 meters may be attributed in part to the use of a sophisticated gravity model (SAO M-1 model—Reference 2) and the transformation of all tracking site locations to a datum (SAO C-5—Reference 2) using the center of mass of the earth as its origin and consistent with the gravity model used.

FEASIBILITY OF USING OPTICALLY-DETERMINED "STANDARD ORBITS" TO EVALUATE AND CALIBRATE MINITRACK DATA

The feasibility of using optical observations of artificial satellites for calibration purposes has been previously noted by V. R. Simas.* The large volume of high-precision optical observations of GEOS I currently available offers the first opportunity to analyze in depth the data obtained from the Minitrack network of the same satellite and to explore the feasibility of utilizing such optical data for calibration purposes. As noted in Appendix A, the upper precision limit obtainable at the most basic level of the electronics of the Minitrack system (the phase-measurement level) is about 0.36 electrical degrees. This is equivalent to a precision of approximately 5" in terms of ability to measure angular arc in space under optimum conditions at the zenith. A more realistic figure for the overall expected precision of the Minitrack system at the equipment level is probably around 20" in terms of angular direction in space (Reference 3, p. 84). The precision of the SAO optical observations is estimated to be approximately 2" (Reference 2, p. 43) for a single observation. Observations from the MOTS, PC-1000, and other cameras used in the GEOS I program have an inherent precision which is slightly better than the SAO figure. Whether or not this inherently greater accuracy is actually realized will depend to a great extent upon the care exercised in reducing and preprocessing the data. Taking the SAO figure of 2" as an approximate gauge of the overall accuracy of an individual optical observation, there is sufficient justification for using optical observations as a standard to be used in analyzing and evaluating Minitrack network data provided that there exist no significant systematic differences between the two data types. In a later section, this will be shown to be the case when considering the Minitrack network as a whole, although there appear to be systematic problems at individual Minitrack sites. Even if there exist significant systematic differences between the two data types, there still is a strong justification for using optical data as a "standard," since all detectable error sources in this data type as exist in star catalogues, plate measuring equipment, optical refraction, etc., have had the advantage of decades of thorough study by competent investigators, so that the error limits of these sources are well known.

*Unpublished notes, Sections 3.4.4 and 3.4.5, p. 54.

A certain amount of caution should be exercised when considering the MOTSOptical observations as used in the "standard orbit," since the MOTScameras are used also for calibrating the Minitrack system and any undetected systematic errors in the MOTS instrumentation will probably be propagated into the Minitrack calibration coefficients. However, since the MOTScameras are co-located with the center of the Minitrack antenna "fine beam" array, these optical observations may prove useful in verifying suspected systematic errors which have been detected by the Minitrack residuals.

One particularly useful conclusion of the current investigation is that an optically-determined "standard orbit" has great value in detecting systematic errors at individual Minitrack sites. If these individual systematic errors can be identified and removed, the overall result will be a corresponding reduction in the rms of fit of orbits as determined by Minitrack data only. It is suggested also that the use of an optically-determined "standard orbit" would be a preferable method of calibrating the individual Minitrack sites. The current method of calibration by means of simultaneously photographing an airborne flashing light with the MOTS cameras and detecting the 136.5-Mc radio signal with the Minitrack antenna arrays is not capable of detecting all systematic errors. Some obvious examples are errors in site location and timing errors. At best, the present calibration method can account only for local systematic errors.

SUMMARY OF OPTICAL DATA USED IN THE "STANDARD ORBIT" SOLUTION

The GEOS I optical and Minitrack data used in the analysis described in this report were obtained from the NASA Space Science Data Center located at the Goddard Space Flight Center.

The "standard orbit" used in the calculation of the Minitrack residuals in the current analysis was determined completely from optical observations of GEOS I. Minitrack observations were not used to adjust the standard orbit which was used as a basis for the calculation and subsequent analysis of the Minitrack residuals.

For the purpose of calibrating electronic equipment, the "active" GEOS I optical data are particularly useful as a high-precision data set. In addition to the reasons noted earlier, other factors contributing to this precision are:

1. The use of a stable on-board clock to trigger the optical beacon flash sequences permitted the determination of the time of observation to millisecond accuracy.
2. The short duration (approximately 1.3 milliseconds) of the optical beacon flash sequences permitted the tracking cameras to record the observations as point images rather than as a streak against a background of reference stars, thus making it possible for the right ascensions and declinations of the flashes to be determined to higher precision than normally obtained.

In general, the reduction methods associated with using reference stars as a means of determining angular position are the most accurate available among all current tracking systems.

The epoch of the standard orbit was 01^h 38^m 22^s.000 12/31/1965 UTC time. The epoch was chosen at the beginning of the selected optical data set which extended to 06^h 45^m 1^s/5/1966 UTC, a total arc length of approximately 5-1/4 days covering 63 orbital revolutions of the spacecraft. The resulting rms of fit of this particular standard orbit was 3".12 based upon 1059 observations summarized in Table 1.

Table 1

Summary of GEOS I Optical Observations Used in the Orbital Solution
for the Period 1^H 38^M 12/31/65 or 6^H 45^M 1/5/66 (63 Orbital Revolutions).

Network	Station	Camera Type	No. of Observations				
			α	δ	α and δ	Type	No. Passes/ No. Flash Seq.
SAO	1ORGAN	Baker-Nunn	1	1	2	Passive	1/
	1MAUIO	Baker-Nunn	1	1	2	Passive	1/
	1NATOL	Baker-Nunn	4	4	8	Passive	4/
	OSLONR	Baker-Nunn	2	2	4	Passive	2/
	AUSBAK	Baker-Nunn	2	2	4	Passive	2/
	1SHRAZ	Baker-Nunn	1	1	2	Passive	2/
	1SPAIN	Baker-Nunn	3	3	6	Passive	3/
	1TOKYO	Baker-Nunn	6	6	12	Passive	6/
	1VILDO	Baker-Nunn	1	1	2	Passive	1/
	1JUPTR	Baker-Nunn	14	14	28	Active	1/2
	AGASSI	K-50	5	5	10	Active	1/1
	TOTAL		40 + 40 = 80 (21 + 21 = 42 total passive)				
SPEOPT	1COLBA	MOTS 40"	81	83	164	Active	8/13
	1JUM40	MOTS 40"	7	15	22	Active	3/3
	1BERMD	MOTS 40"	39	45	84	Active	5/7
	1PURIO	MOTS 40"	7	7	14	Active	1/1
	1DENVR	MOTS 40"	28	42	70	Active	4/6
	1JUM24	MOTS 40"	10	16	26	Active	3/3
	TOTAL		172 + 208 = 380			Active	
STADAN	1FTMYR	MOTS 40"	41	41	82	Active	4/6
	1BPOIN	MOTS 40"	23	30	53	Active	5/6
	1GFORK	MOTS 40"	11	15	26	Active	3/3
	1MOJAV	MOTS 40"	12	13	25	Active	2/2
	TOTAL		87 + 99 = 186				
USAF	HUNTER	PC-1000	30	29	59	Active	5/5
	SWANIS	PC-1000	7	7	14	Active	1/1
	GRDTRK	PC-1000	0	7	7	Active	1/1
	ANTIGA	PC-1000	13	13	26	Active	2/2
	SEMMES	PC-1000	30	30	60	Active	4/5
	CURACO	PC-1000	20	20	40	Active	3/3
	HOMEST	PC-1000	47	47	94	Active	4/6
	JUPRAF	PC-1000	12	5	17	Active	2/2
	BEDFRD	PC-1000	11	11	22	Active	2/2
	ABERDN	PC-1000	37	37	74	Active	6/6
	TOTAL		207 + 206 = 413				21/ Passive 70/86 Active

Total of All Observations = 1059
Total Passive Observations = 42

91 Total Station-Passes

A more detailed description of the names, general locations, and specific coordinates of the tracking stations corresponding to the adopted six-character station code names listed in Table 1 and other tables and figures of this report is given in Appendix D. The position and velocity vectors for the epoch 01^H 38^M 22^S.000 12/31/1965 UTC which were adjusted on the basis of the 1059 optical observations are given in Table 2. A summary of optical data coverage by time is shown in Figure 1.

Table 2

Final Adjusted Position and Velocity Vectors at Epoch for the Optical "Standard Reference Orbit."

Optically Adjusted Position Vector		Optically Adjusted Velocity Vector	
X:	+5,690,537.7 meters	\dot{X} :	-4,685.6198 meters/sec.
Y:	+1,474,538.5 meters	\dot{Y} :	+3,849.4695 meters/sec.
Z:	+6,013,442.9 meters	\dot{Z} :	+2,939.1210 meters/sec.
Epoch:	01 ^H 38 ^M 22 ^S .000 12/31/1965 UTC		
No. of Observations:	1059		
Arc Length:	5-1/4 days		
Rms of Fit:	3".12		

For comparable arc lengths, this rms of fit was not of the highest quality. A more typical figure for GEOS I for this arc length would be approximately 2".0. However, this particular arc had been used for intercomparison with other instrumentation types and it was felt that a multiple-instrument intercomparison would prove useful. In addition, the 3".12 rms of fit still places the optical data set well within the precision limits required for a Minitrack intercomparison.

The 1059 optical observations are summarized in Table 1 by network, station, and type, i.e., whether the data were active or passive. In addition, a further breakdown is given of the active observations according to the number of passes over a particular station and the total number of flash sequences (maximum of 7 right ascensions and 7 declinations per flash sequence) per station. These data are more

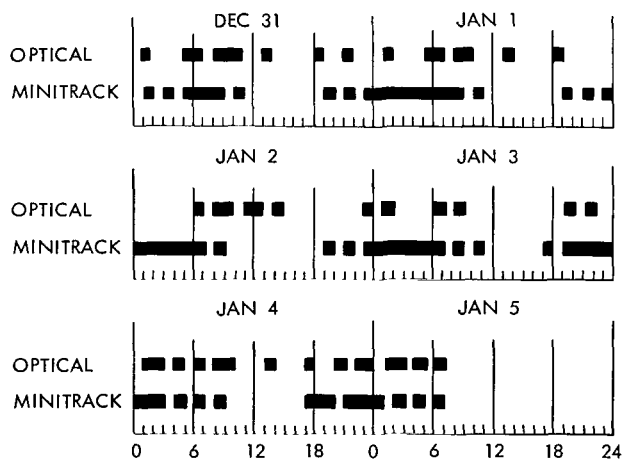


Figure 1—Summary of GEOS I optical and Minitrack coverage for the period 01^H 38^M 12/31/65 to 06^H 45^M 1/5/66 UTC (63 orbital revolutions).

descriptive of the available station coverage and geometrical strength if they are described in terms of "station-passes."

The final tally reduces the total of 1059 optical observations to 86 active flash sequences during 70 "active station-passes" over the various optical stations and 21 "passive station-passes." The total number of "station-passes" was 91. The 21 "passive station-passes" were all obtained from the SAO network. Of the 70 "active station-passes," only 2 were obtained from the SAO network. The remaining 68 "active station-passes" were distributed as follows:

- 30 passes USAF Network PC-1000 cameras
- 24 passes SPEOPT Network MOTS 40" cameras
- 14 passes STADAN Network MOTS 40" cameras

The 68 passes from the Air Force, SPEOPT, and STADAN networks were all located on the North American continent or its near vicinity (Figure 2). In addition, the only two "active station-passes" from SAO, at Agassiz, Massachusetts, and Jupiter, Florida, are on the North American continent (Figure 3). At least one station-pass was obtained from every SAO station shown in Figure 3 except Olifantsfontein in South Africa. The rms of fit of 3".12 for the 5-1/4 days of optical observations was obtained using the SAO M-1 gravity model modified by the GEOS I resonant

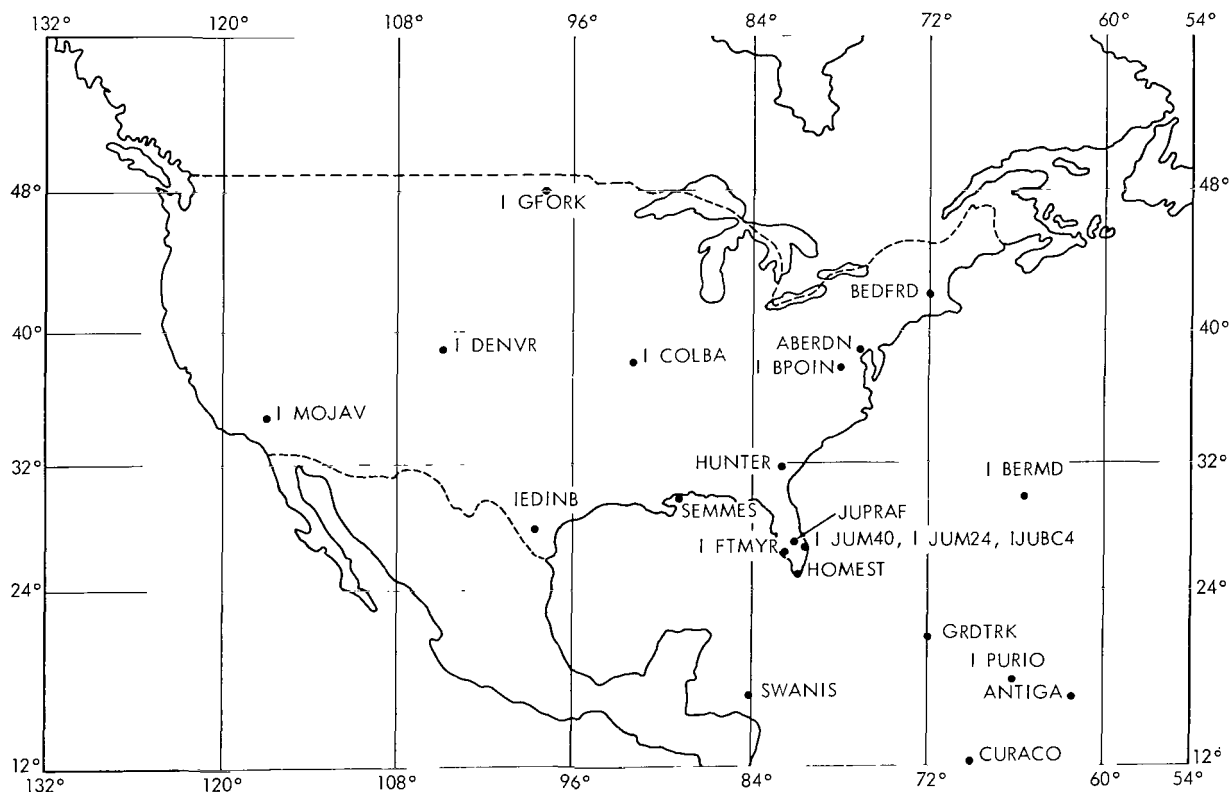


Figure 2—Location of USAF, SPEOPT, and STADAN camera sites whose observations were used in the orbital solution.

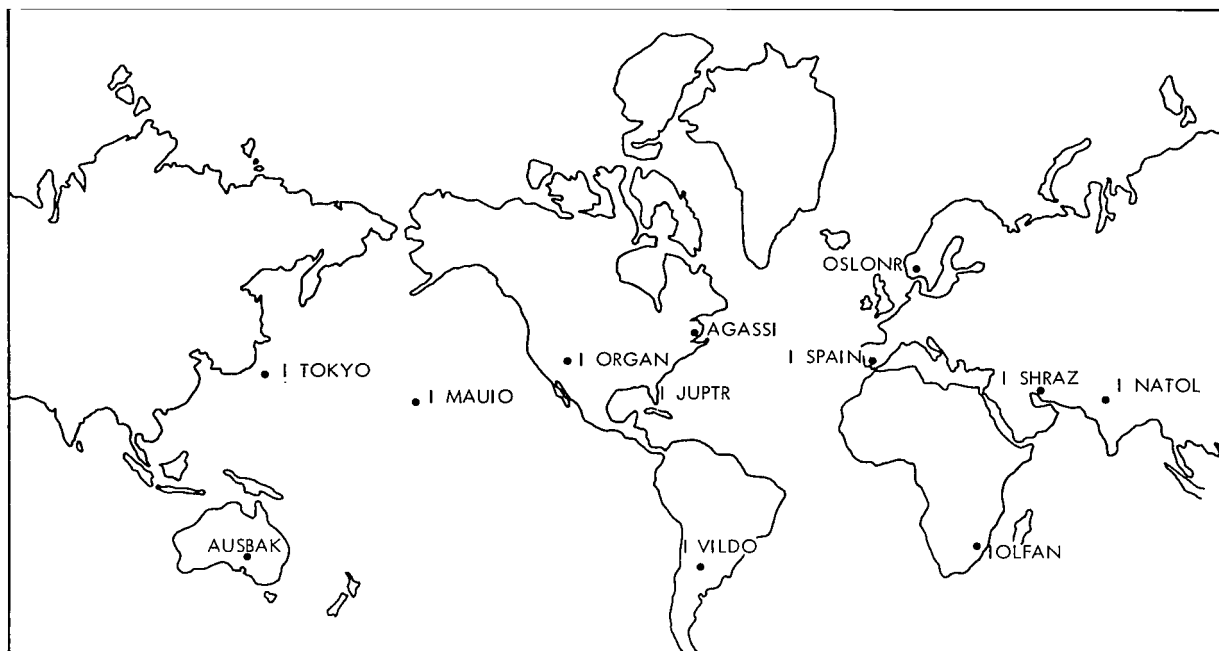


Figure 3—SAO Baker-Nunn camera site locations.

harmonics ($C_{13.12}$, $C_{14.12}$, $C_{15.12}$, $S_{13.12}$, $S_{14.12}$, $S_{15.12}$) as redetermined by SAO (Reference 2, p. 2; Reference 4, p. 5; and Appendix C). All tracking station locations were transformed to the SAO C-5 system (Reference 2, p. 2; Appendix D).

SUMMARY OF MINITRACK DATA AVAILABLE FROM THE SPACE SCIENCE DATA CENTER FOR THE PERIOD OF INTEREST, AND DATA REJECTED BEFORE ANALYSIS

The Minitrack data as obtained from the NASA Space Science Data Center consist of 1 to 3 pairs of direction cosines per station-pass. These data in turn have been reduced by Goddard from approximately 30 pairs of phase-difference measurements per pass as transmitted to Goddard from the various Minitrack stations. Goddard transforms these data to direction cosines and reduces them to approximately 1 to 3 data pairs of direction cosines by means of a polynomial smoothing process. This is the only data preprocessing performed before the data are transmitted to the Space Science Data Center or used by Goddard's own orbit differential correction program. The rms of fit of the polynomial smoothing process is slightly less than 0.1×10^{-3} on the average.*

During normal operations, the Minitrack stations do not track below 20° zenith distance except during early launch phases. In the case of GEOS I, an exception was made and tracking was performed almost to the horizon. For the current analysis, Minitrack observations are available down to 15° elevation, so that there is a sufficient span of data in that dimension to investigate refraction effects.

The Minitrack data originally available for analysis from the Space Science Data Center for the period of interest consisted of 482 observations, summarized by station in the first column of Table 3.

*Watkins, E. R., Jr., private communication, Operational Computing Branch, Computation Division, Goddard Space Flight Center.

Table 3

Summary of Minitrack Data Rejected for Analysis Purposes for the
 Period 1^H 38^M 12/31/65 to 6^H 45^M 1/5/66 (Approximately 63 Orbital Revolutions).

Station	l				m			
	Total No. of Obs. Available	No. of Obs. with Residuals Greater Than 0.5×10^{-3}	Total No. of Obs. Rejected	% of Obs. with Residuals Greater Than 0.5×10^{-3}	Total No. of Obs. Available	No. of Obs. with Residuals Greater Than 0.5×10^{-3}	Total No. of Obs. Rejected	% of Obs. with Residuals Greater Than 0.5×10^{-3}
1. BPOINT	50	1	4	2.0	50	2	4	4.0
2. COLEGE	25	3	4	12.0	25	2	4	8.0
3. FTMYRS	21	2	4	9.5	21	3	4	14.3
4. GFORKS	29	2	2	6.9	29	1	2	3.4
5. JOBURG	2	0	0	0.0	2	0	0	0.0
6. LIMAPU	6	0	0	0.0	6	0	0	0.0
7. MOJAVE	38	1	2	2.6	38	1	2	2.6
8. NEWFLD	38	0	2	0.0	38	1	2	2.6
9. OOMERA	6	1	2	16.7	6	1	2	16.7
10. QUITOE	4	0	0	0.0	4	0	0	0.0
11. SNTAGO	4	0	0	0.0	4	0	0	0.0
12. WNKFLD	18	3	3	16.7	18	2	3	11.1
<i>l</i>	241	13	23	5.4%	241	13	23	5.4%
<i>m</i>	241	13	23	5.4%				
TOTAL	482	26*	46	5.4%				

*5.4% of data.

After a rejection criterion (described in the next paragraph) was applied to the data, 436 data points remained for the analysis. These data are summarized in Table 4. The 436 data points comprise 158 station-passes, compared to the 91 station-passes of optical data (Table 1). For the Minitrack data also, the geometry is strongly oriented toward the North American continent, with 29 passes at Blossom Point, Maryland, 26 passes at St. John's, Newfoundland, and 25 passes at Mojave, California. At least one observation pair was obtained from every Minitrack station (Figure 4) except the one located at Tananarive.

A cutoff criterion of 0.5×10^{-3} in direction cosine residuals was used in the rejection of data to be used in the analysis. This particular figure was chosen for convenience in the analysis of the residuals and to correspond to approximately 2-1/2 times the rms of the orbital fit. For data

Table 4

Summary of Minitrack Observations Used in Intercomparisons for the Period 1^H 38^M 12/31/65 to 6^H 45^M 1/5/66 (Approximately 63 Orbital Revolutions).

Station	No. of Observations			Location
	ℓ	m	No. of Passes	
1. BPOINT	46	46	29	Blossom Point, Maryland
2. COLEGE	21	21	18	College, Alaska
3. FTMYSRS	17	17	12	Fort Myers, Florida
4. GFORKS	27	27	19	East Grand Forks, Minnesota
5. JOBURG	2	2	2	Johannesburg, South Africa
6. LIMAPU	6	6	4	Lima, Peru
7. MOJAVE	36	36	25	Mojave, California
8. NEWFLD	36	36	26	St. John's, Newfoundland
9. OOMERA	4	4	4	Woomera, Australia
10. QUITOE	4	4	3	Quito, Ecuador
11. SNTAGO	4	4	4	Santiago, Chile
12. WNKFLD	15	15	12	Winkfield, England
TOTAL	218	+	218	158 Total Station-Passes = 436

Rms orbital fit using Minitrack data only = 0.19×10^{-3} .

All Minitrack data rejected whose residuals from optically-determined orbit exceeded 0.5×10^{-3} (5% of smoothed data available from data center).

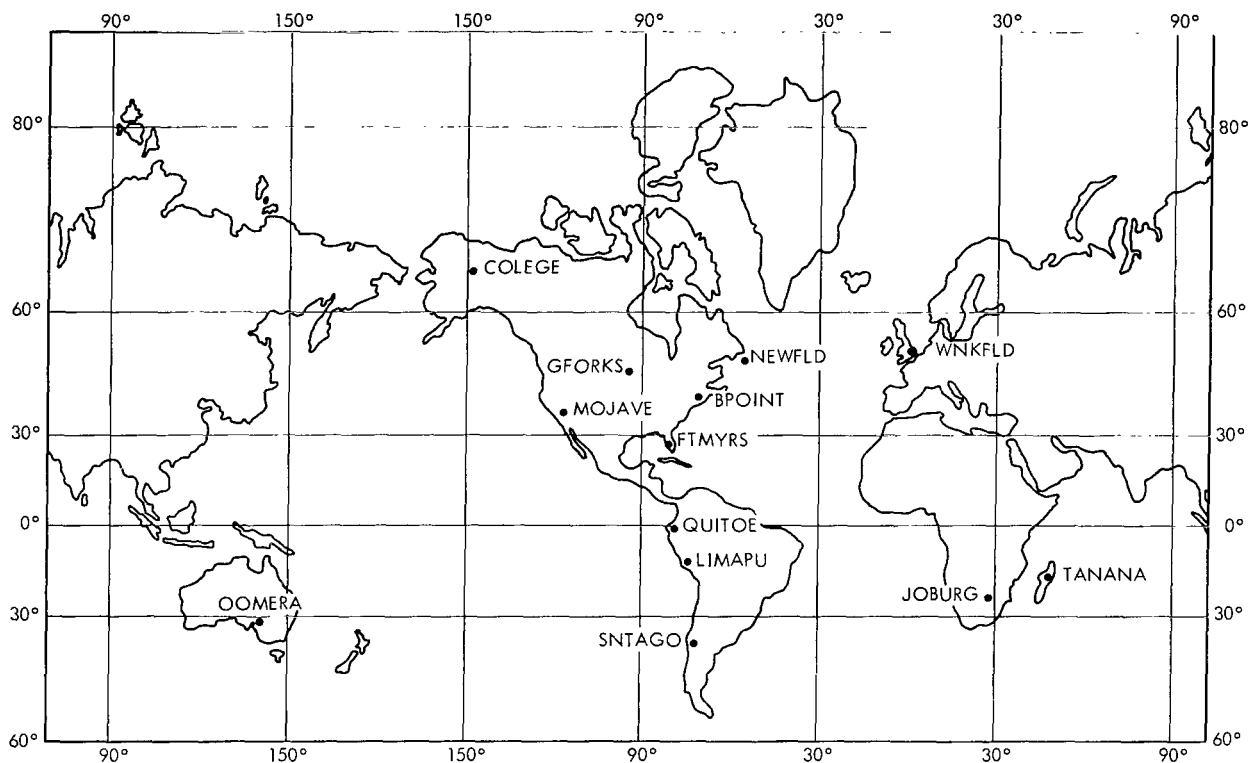


Figure 4—STADAN 136-Mc Minitrack interferometer site locations.

rejection purposes also, the "standard orbit" was used as the basis for calculating the Minitrack residuals.

Approximately 5 percent of all Minitrack data available from the NASA Space Science Data Center during the period of analysis exceeded this figure. Thus the percentage of data rejected on the basis of the 0.5×10^{-3} cutoff criterion is statistically consistent with the assumption of a normal distribution of the residuals (see residual plot in Figure 7). Minitrack data rejected on the basis of this criterion are summarized by station in Table 5. The magnitude of the residuals enclosed by rectangles in this table was less than the criterion, but they were omitted from the analysis because their counterpart exceeded the criterion. One residual pair from Blossom Point, Maryland, at 17° elevation was erroneously rejected because of a faulty computer printout on the first pass through the data. A final summary of the total number of original observations and number of observations rejected by station is shown in Table 3. The total number of observations rejected from the analysis was 46 of a total of 482, or 9-1/2 percent of the total data available. This is higher than the 5.4 percent of the data which actually exceeded the rejection criterion of 0.5×10^{-3} , because both data points of a pair were rejected even though only one of the two points may have exceeded the criterion. The rejection of 16.7 percent of the data from Woomera, Australia, is statistically insignificant because of the small number of observations available from that station (6 pairs). Of perhaps more significance is the 10 percent rejection rate for College, Alaska. It will be shown later that there is a strong bias in the residuals from this station which may account for the high rejection rate.

Table 5

Table of Residuals of Minitrack Data Rejected for Analysis Purposes
(Rejection Criterion— 0.5×10^{-3}).

Station	Δl	Δm	Elevation
GFORKS	2.54×10^{-3}	1.74×10^{-3}	71°
	6.02×10^{-3}	$\boxed{.07} \times 10^{-3}$	44
BPOINT	507.12×10^{-3}	452.86×10^{-3}	-56
	$\boxed{.19} \times 10^{-3}$	$.61 \times 10^{-3}$	23
	$\boxed{.03} \times 10^{-3}$	$\boxed{.06} \times 10^{-3}$	17
	$\boxed{.29} \times 10^{-3}$	$.83 \times 10^{-3}$	21
COLEGE	18.15×10^{-3}	$\boxed{.30} \times 10^{-3}$	23
	17.97×10^{-3}	23.78×10^{-3}	20
	17.40×10^{-3}	17.56×10^{-3}	19
	$.51 \times 10^{-3}$	$\boxed{.15} \times 10^{-3}$	28
FTMYRS	$.74 \times 10^{-3}$	$\boxed{.09} \times 10^{-3}$	50
	$.61 \times 10^{-3}$	$.55 \times 10^{-3}$	23
	$\boxed{.27} \times 10^{-3}$	$.58 \times 10^{-3}$	28
	$\boxed{.41} \times 10^{-3}$	$.59 \times 10^{-3}$	27
MOJAVE	17.22×10^{-3}	$\boxed{.06} \times 10^{-3}$	22
	$\boxed{.12} \times 10^{-3}$	$.54 \times 10^{-3}$	34
NEWFLD	$\boxed{.23} \times 10^{-3}$	$.52 \times 10^{-3}$	17
	$\boxed{.12} \times 10^{-3}$	$.61 \times 10^{-3}$	70
WNKFLD	132.50×10^{-3}	113.17×10^{-3}	70
	187.89×10^{-3}	47.89×10^{-3}	61
	1.99×10^{-3}	$\boxed{.14} \times 10^{-3}$	62
OOMERA	$.62 \times 10^{-3}$	$\boxed{.25} \times 10^{-3}$	47
	$\boxed{.38} \times 10^{-3}$	$.62 \times 10^{-3}$	63

Any residual enclosed by a rectangle (except the BPOINT residuals at 17° elevation) is less than the rejection criterion but was omitted from the analysis because its counterpart exceeded the criterion. Although both BPOINT residuals at 17° elevation were less than the rejection criterion, they were erroneously rejected.

An orbit is described later (in the last section of this report before "Conclusions") which is adjusted on the basis of Minitrack data only. These data were not corrected for tropospheric or ionospheric refraction effects and were not weighted for elevation effects in the orbital adjustment process. The resulting rms of fit was 0.19×10^{-3} . It is significant that when the Minitrack residuals were recalculated on the basis of the same orbital arc as adjusted by Minitrack data only, there were no additional residuals encountered falling outside the 0.5×10^{-3} criterion originally used to reject Minitrack residuals calculated on the basis of the "standard orbit."

GEOMETRY OF THE MINITRACK "EQUATORIAL" AND "POLAR" MODES OF TRACKING

The 136-Mc Minitrack interferometer tracking system and its tracking geometry are described in Appendix A. The tracking geometry is summarized in Figure 5. There are two possible modes of tracking, the "equatorial" tracking mode and the "polar" tracking mode. In the equatorial mode,

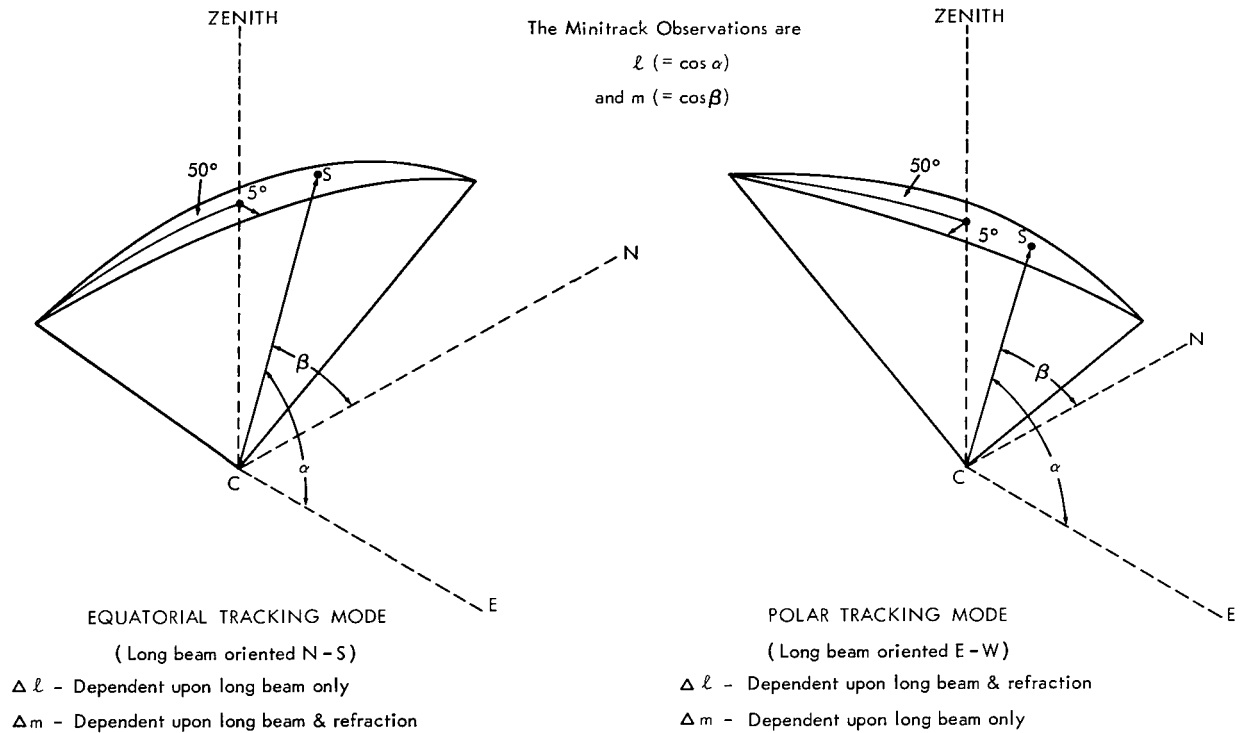


Figure 5—Approximate reception pattern of the fine beam of the 136-Mc Minitrack antenna array in the equatorial and polar tracking modes.

the "fine beam" is oriented in a north-south direction, with the long portion of the beam stretching 50° on each side of the zenith and 5° on each side of the zenith in the east-west direction relative to the station center C. When tracking in the polar tracking mode, the long portion of the "fine beam" is oriented east-west and the narrow portion oriented north-south. The particular mode of tracking is usually determined by the direction in which the satellite is approaching the station. It is possible to switch electronically from one mode to the other fairly quickly. Several passes of GEOS I during the period of analysis were tracked in both modes during the same pass.

The observations available as data are the direction cosines l and m , which are equal respectively to the cosines of the angles α and β as indicated in Figure 5. A vector directed toward the satellite is indicated in this figure in both the equatorial and polar tracking modes. Observational data are usually available only when the satellite is located inside this fan-shaped fine beam, although there are occasional data outside this pattern in the "side lobes." Observations made within the fine beam are considered to be more accurate than observations made in the side lobes.

The method of obtaining calibration coefficients for the individual Minitrack stations is described in References 5 through 8. The method employed by Goddard Space Flight Center in transforming the raw Minitrack phase measurements to direction cosines, making use of these calibration coefficients and other relevant information, is described in References 9 through 12

and 13a, b, and c.* The corrections for ionospheric and tropospheric refraction as employed by the operational orbit determination program are described in References 14a and b and 15.

Refraction corrections were not applied to the measurements used in the analysis performed in this report, as mentioned also in the preceding section.

The Minitrack antenna arrays are laid out by a method of leveling corresponding to the astronomical zenith. The raw phase measurements are referenced to an "electrical" zenith defined by the antenna system. However, the calibration equations referred to above transform the raw phase measurements to direction cosines relative to the geodetic zenith.

USE OF THE MINITRACK GEOMETRY TO UNCOUPLE REFRACTION-DEPENDENT FROM REFRACTION-INDEPENDENT EFFECTS IN THE MINITRACK RESIDUALS

By considering the geometry of the antenna pattern in Figure 5 more closely, it is seen that, in the equatorial tracking mode, the angle α will never be less than 85° or more than 95° and the angle β will be approximately equal to the elevation angle or its supplement. In the polar tracking mode, the situation is reversed and β will always be between 85° and 95° and α will be approximately equal to the elevation angle or its supplement. For the purposes of the analysis in this report, it will be assumed on the basis of this configuration that any systematic errors due to refraction are not present in $\Delta \ell_{eq.}$ and Δm_{polar} , ($\Delta \ell_{eq.}$ = residuals in the direction cosine ℓ when tracking in the equatorial tracking mode; Δm_{polar} = residuals in the direction cosine m when tracking in the polar tracking mode). Whatever systematic effects may be present in $\Delta \ell_{eq.}$ and Δm_{polar} will be called a "beam only" effect. It will be assumed that $\Delta \ell_{polar}$ and $\Delta m_{eq.}$, i.e., the residuals in the direction cosine ℓ when tracking in the polar tracking mode and in the direction cosine m when tracking in the equatorial tracking mode, will contain both systematic "beam only" effects and systematic "refraction" effects. Any systematic effects which may be due to position across the narrow part of the beam will be neglected.

CONSIDERATION OF RESIDUALS FROM THE MINITRACK NETWORK AS A WHOLE

The Minitrack residuals were calculated on the basis of the 5-1/4-day standard orbit described under "Summary of Optical Data Used in the 'Standard Orbit' Solution." In order to determine the best method of detecting possible systematic trends, the residuals were analyzed by considering the various possible methods of combining $\Delta \ell$ and Δm . Histograms for the entire set of residuals from all 12 stations are shown in Figure 6, with $\Delta \ell$ and Δm together and separately. There is no obvious evidence from these histograms to suggest any strong systematic differences between the optical data and the Minitrack data considered as a whole. No distinction has been made at this point according to the Minitrack mode of tracking (i.e., equatorial or polar).

The residuals which were the basis of the histograms depicted in Figure 6 were then grouped according to the mode of tracking. These results are displayed in Figure 7 in the form of

*See also Simas, V. R., and Watkins, E. R., Jr., as cited in earlier footnotes.

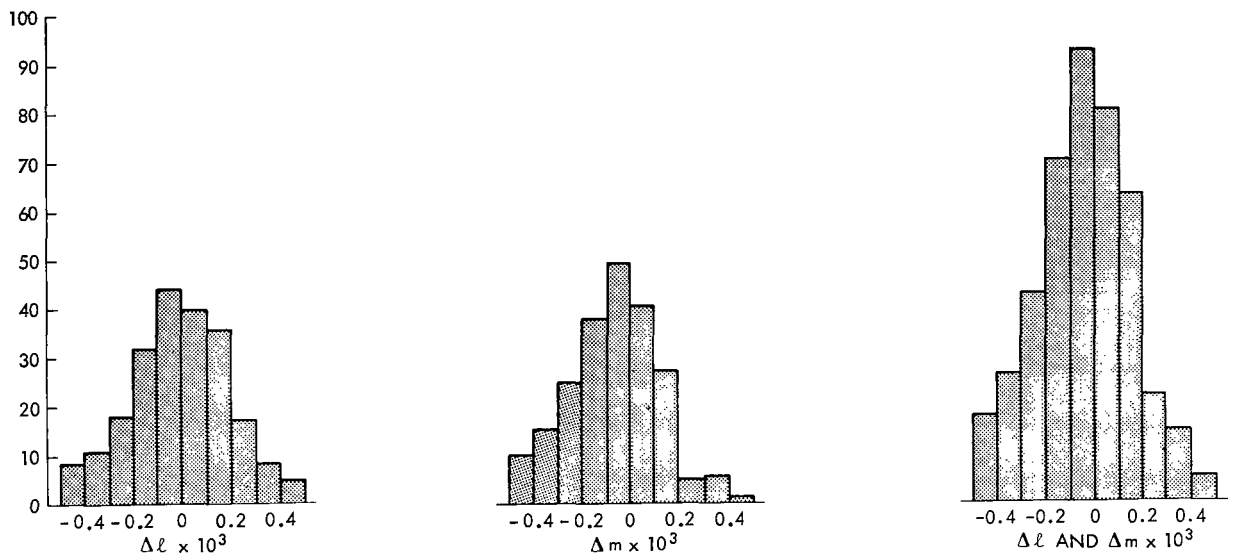


Figure 6—Histograms of Minitrack residuals calculated from optically-determined "standard orbit"—summary from all stations.

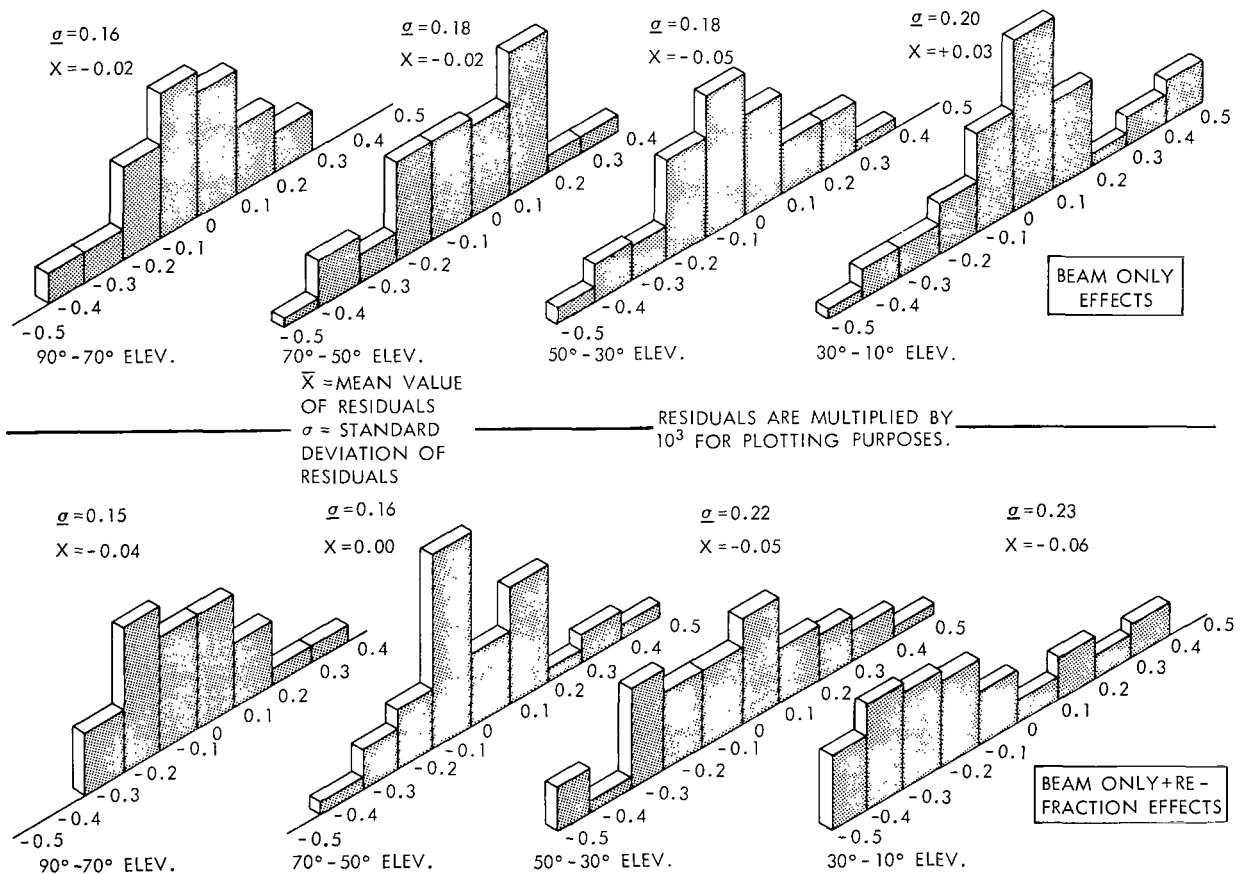


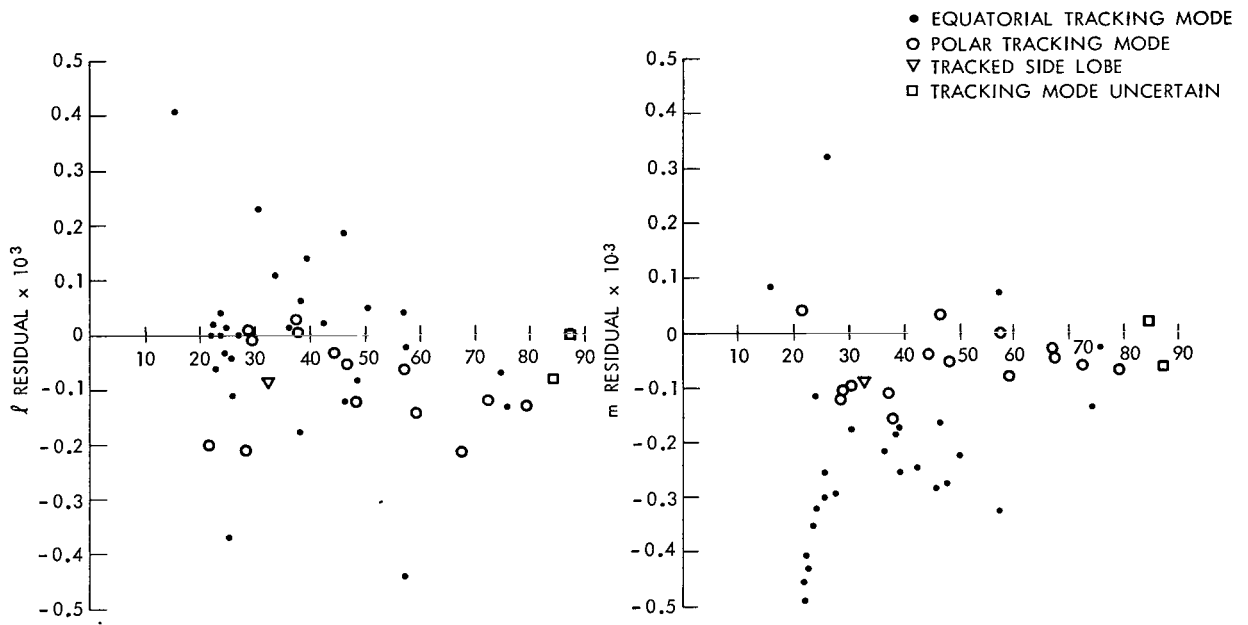
Figure 7—Histograms of Minitrack residuals separated into "beam only" and "beam only + refraction" effects in steps of 20° in elevation angle.

three-dimensional histograms showing relative frequency of magnitudes of the residuals in steps of 0.1×10^{-3} and by elevation angle in steps of 20° . The histogram labeled "Beam Only Effects" is obtained from the frequency of $\Delta \ell_{eq.}$ and $\Delta m_{polar.}$. The histogram labeled "Beam Only + Refraction Effects" is obtained from the frequency of $\Delta \ell_{polar.}$ and $\Delta m_{eq.}$ residuals. The mean values and standard deviations of the residuals in the elevation dimension are printed at the top. For the "Beam Only Effects," the mean values in the different elevation dimensions remain fairly close to 0. In the "Beam Only + Refraction Effects" histogram, there is a definite shift of the mean values of the residuals to the negative at low elevations. In the 10° to 30° elevation dimension, the shift amounts to -0.2×10^{-3} . The small magnitude of the mean values of the "Beam Only Effects" set of residuals is further verification of the absence of strong systematic differences between optical and Minitrack data sets. The relatively large values of the standard deviations can be explained on the basis of individual Minitrack station biases. This effect will be shown in the next section.

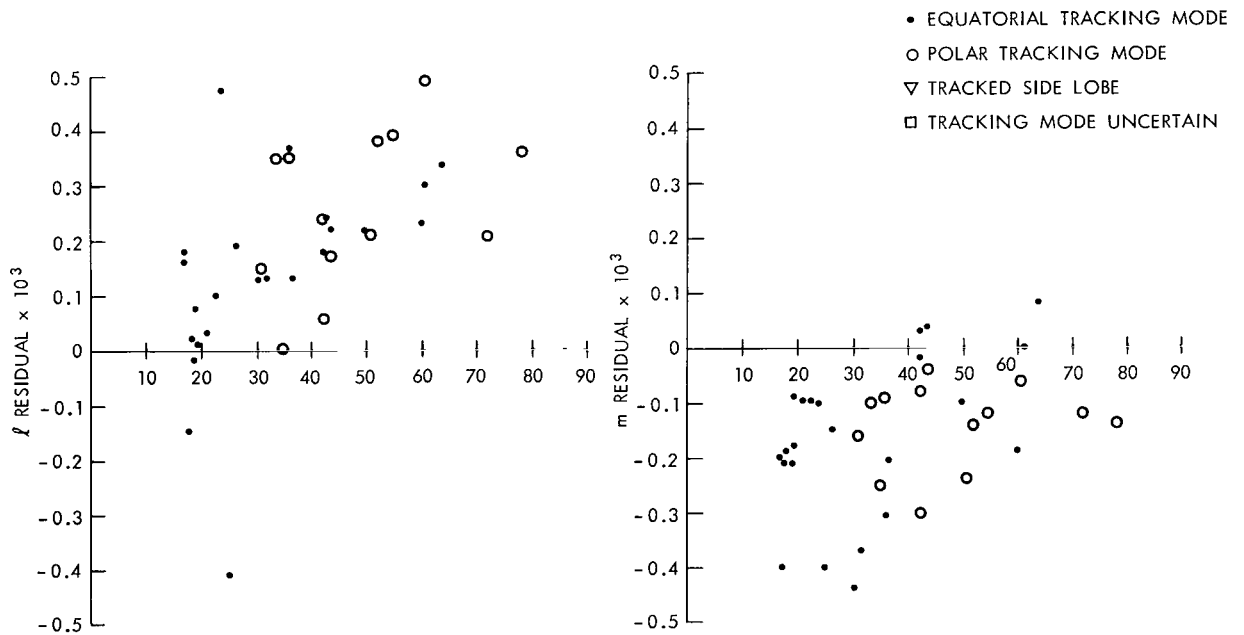
SYSTEMATIC ERRORS AT INDIVIDUAL MINITRACK SITES

In order to detect possible biases at individual Minitrack station sites, the residuals were re-plotted on a station basis. Figures 8a through 8l depict the residuals for each station separately. In these plots by individual station, the ℓ and m direction cosine residuals have been plotted separately as a function of elevation angle. A circle represents a residual obtained from an observation when the equipment was operating in the polar tracking mode. A dot represents a residual obtained from an observation when the equipment was operating in the equatorial mode. This same residual set has been summarized in histogram form in Figures 9a and 9b without regard to tracking mode. There are pronounced biases, particularly at the stations of College, Alaska (COLLEGE), and Mojave, California (MOJAVE). In particular, College has no positive residuals in $\Delta \ell$ and no negative residuals in Δm . At Mojave, there is strong positive bias in the $\Delta \ell$ residuals and a strong negative bias in the Δm residuals.

Considerable caution must be exercised in attempting to analyze residual sets which may or may not contain biases. Also a certain ingenuity is often required in order to unmask and identify these biases if they do exist. For example, the histograms in Figure 6, which summarize the frequency of the Minitrack residuals from all stations both collectively (i.e., $\Delta \ell$ and Δm together) and for $\Delta \ell$ and Δm separately, show no obvious biased tendency even in the separated $\Delta \ell$ and Δm histograms. A rather broad dispersion is evident in this figure, however, both for the case where $\Delta \ell$ and Δm are depicted together and where they are depicted separately. Using a different representation (see Figure 9a), the residuals for some stations now show a strong biased tendency. In this case, the residuals have been separated and depicted by individual station as well as separated into the $\Delta \ell$ and Δm histograms. In this form of presentation, the biases at Mojave and College are pronounced. However, by considering the individual dispersions by $\Delta \ell$ only and Δm only for each station, the dispersions are in general found to be narrower than indicated by Figure 6 (histogram of all stations together). This suggests that if the sources of these systematic errors can be found and eliminated, there should be a corresponding reduction in the standard deviations both for the individual stations and for the collective data set from all stations.

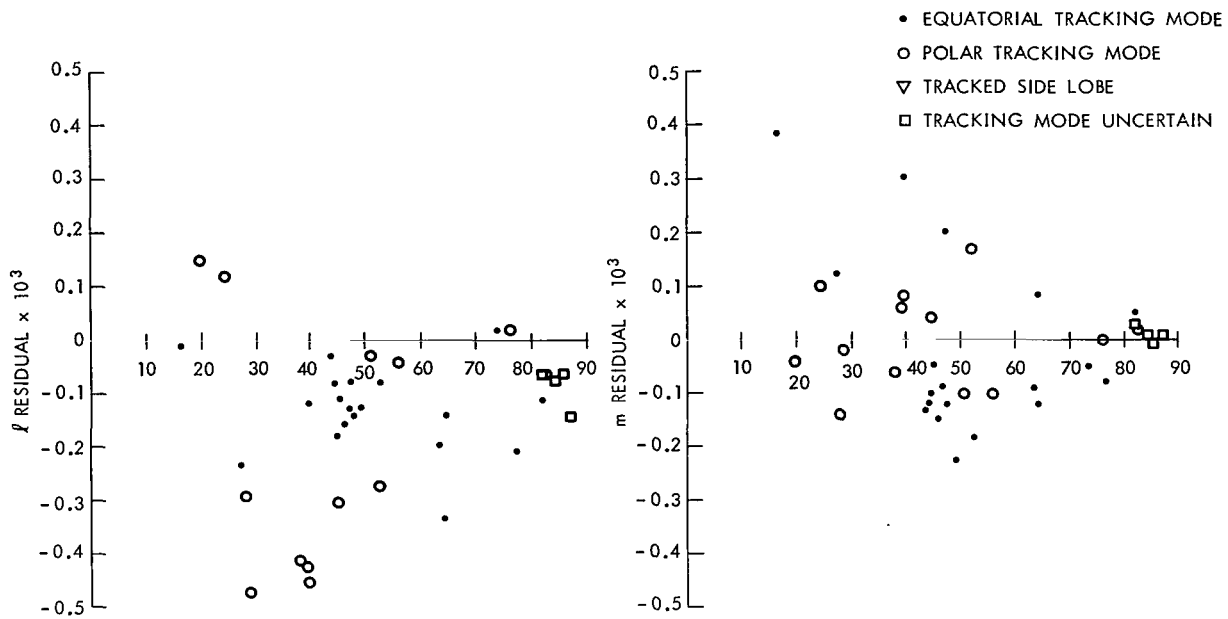


ELEVATION VS DIRECTION COSINE RESIDUAL $\times 10^3$
 a. Blossom Point, Maryland 46 observations

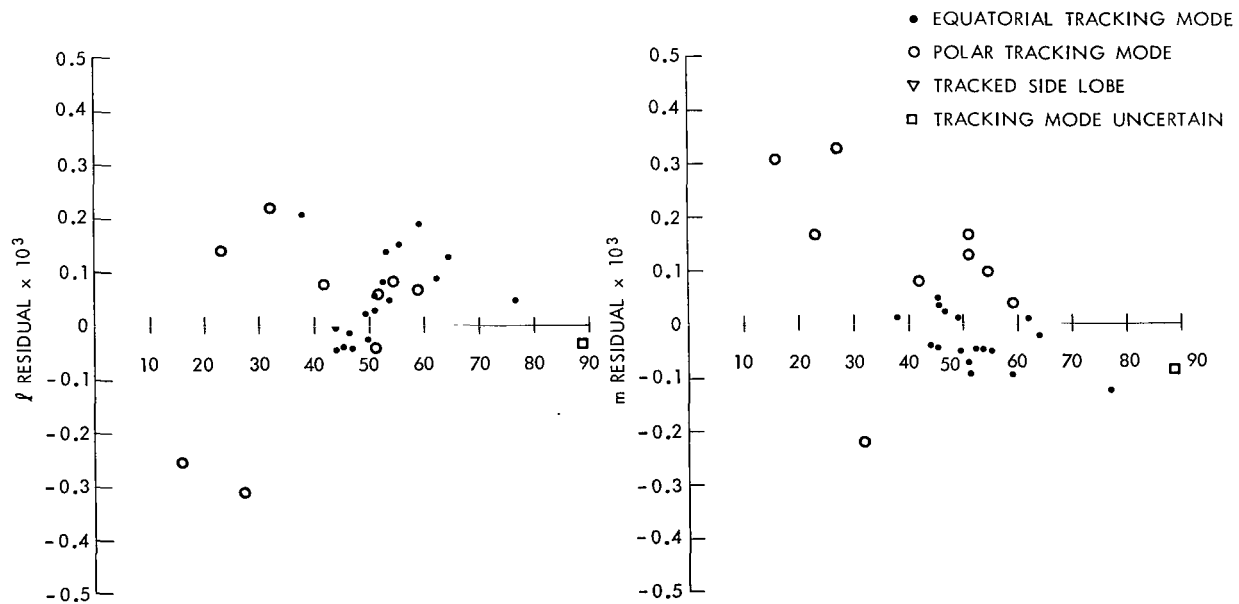


ELEVATION VS DIRECTION COSINE RESIDUAL $\times 10^3$
 b. Mojave, California 36 observations

Figure 8—Plots of elevation vs direction cosine residuals (elevation vs $\Delta l \times 10^3$ and elevation vs $\Delta m \times 10^3$) and mode of tracking (polar or equatorial).

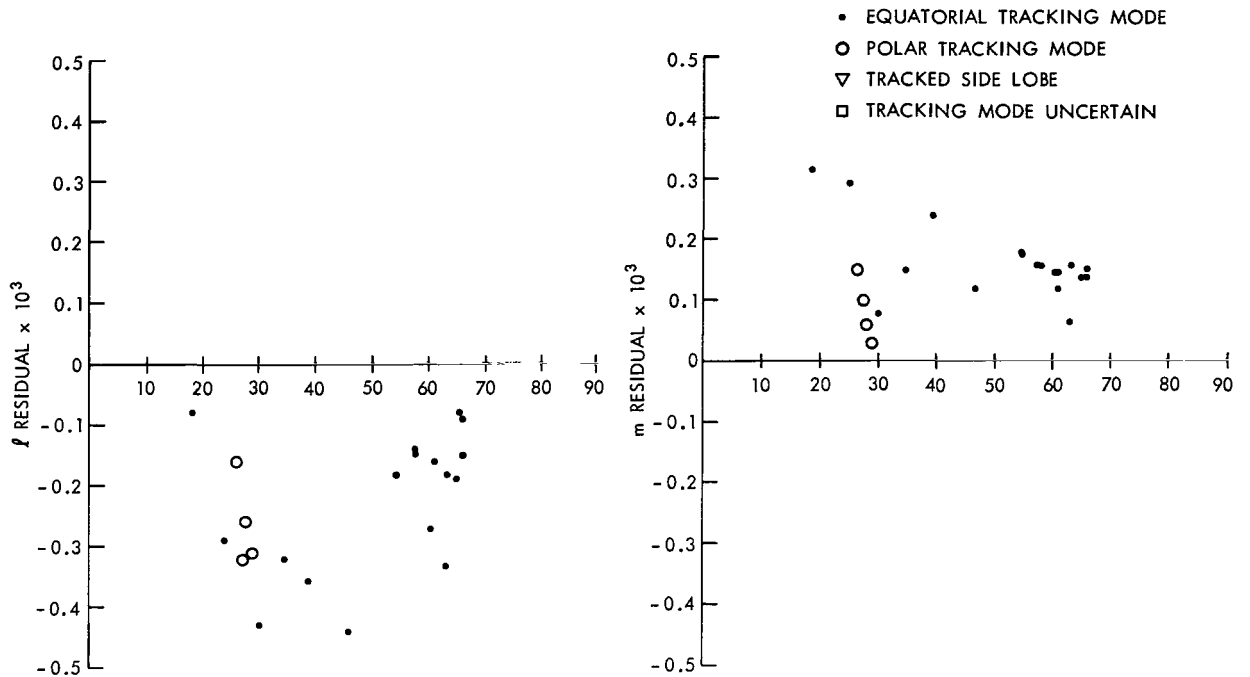


ELEVATION VS DIRECTION COSINE RESIDUAL $\times 10^3$
 c. St. John's, Newfoundland 36 observations

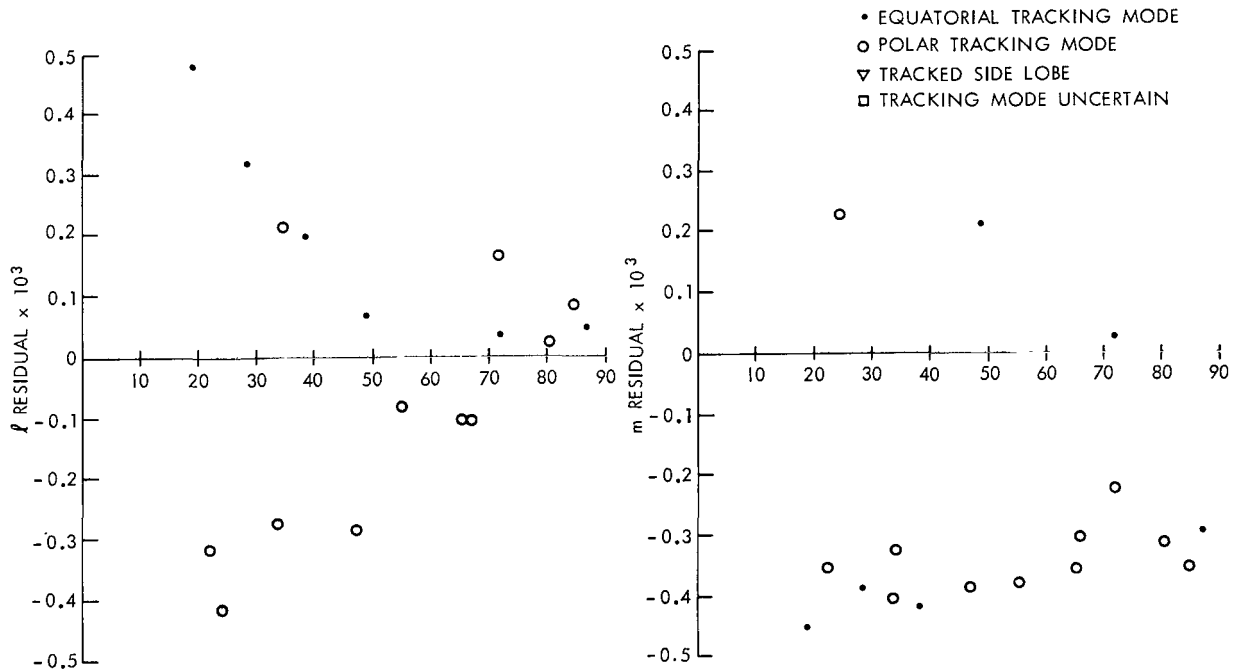


ELEVATION VS DIRECTION COSINE RESIDUAL $\times 10^3$
 d. East Grand Forks, Minnesota 27 observations

Figure 8—Plots of elevation vs direction cosine residuals (elevation vs $\Delta\ell \times 10^3$ and elevation vs $\Delta m \times 10^3$) and mode of tracking (polar or equatorial).

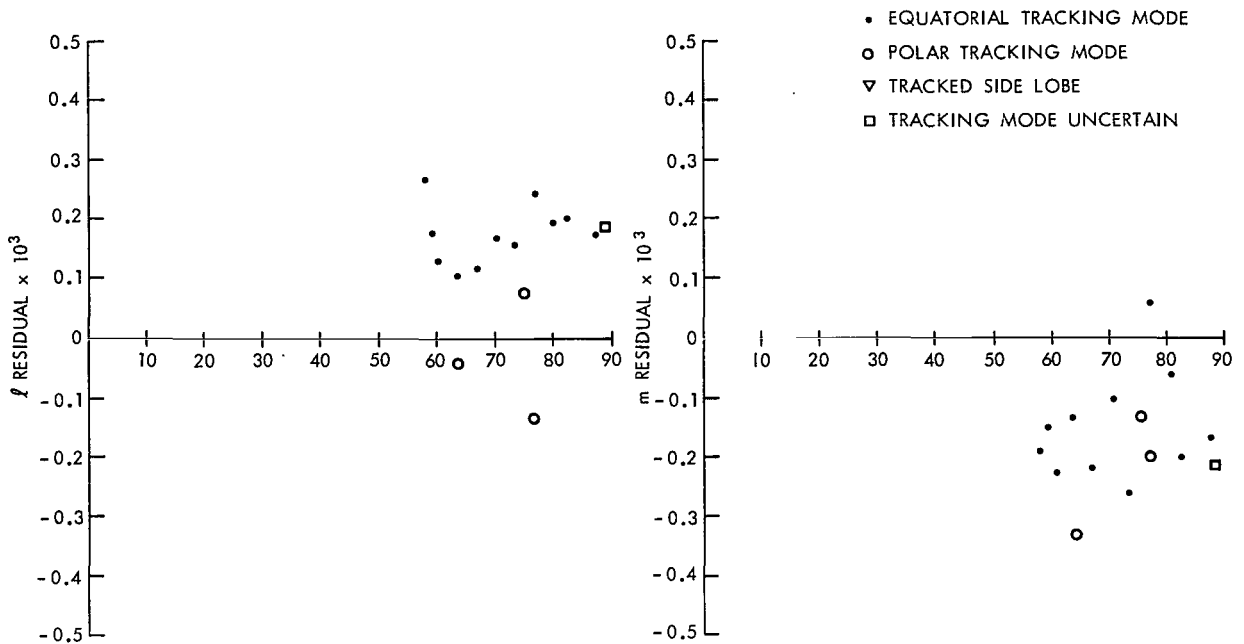


ELEVATION VS DIRECTION COSINE RESIDUAL $\times 10^3$
 e. College, Alaska 21 observations

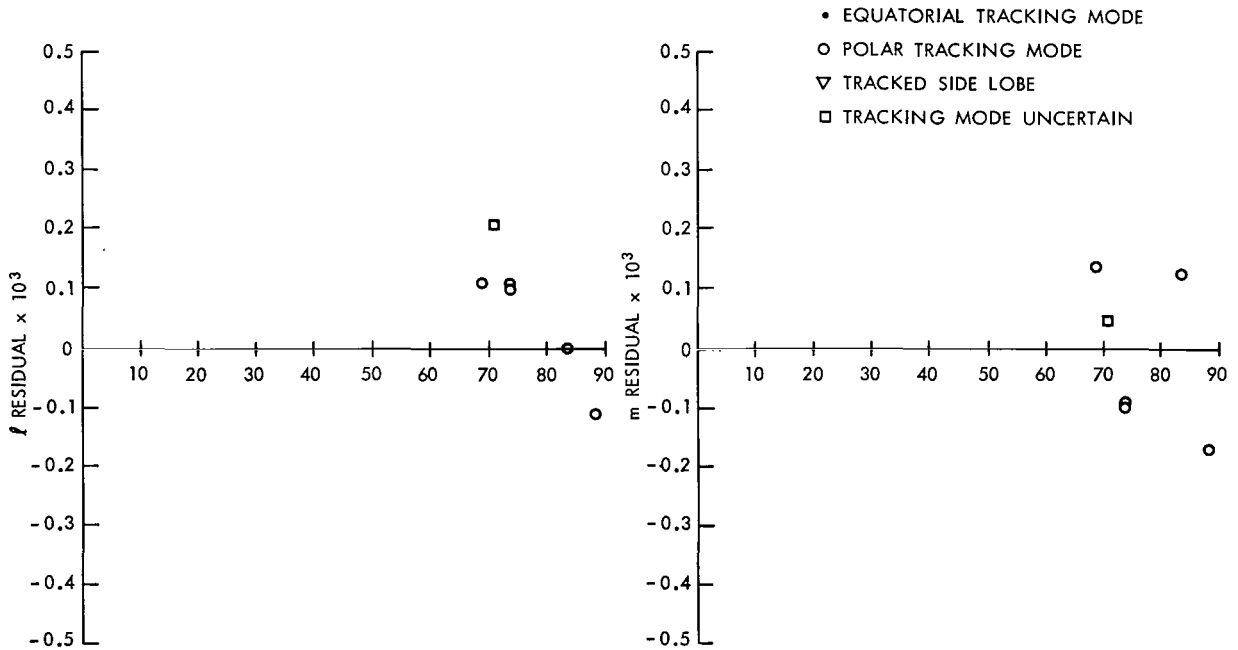


ELEVATION VS DIRECTION COSINE RESIDUAL $\times 10^3$
 f. Fort Myers, Florida 17 observations

Figure 8—Plots of elevation vs direction cosine residuals (elevation vs $\Delta l \times 10^3$ and elevation vs $\Delta m \times 10^3$) and mode of tracking (polar or equatorial).

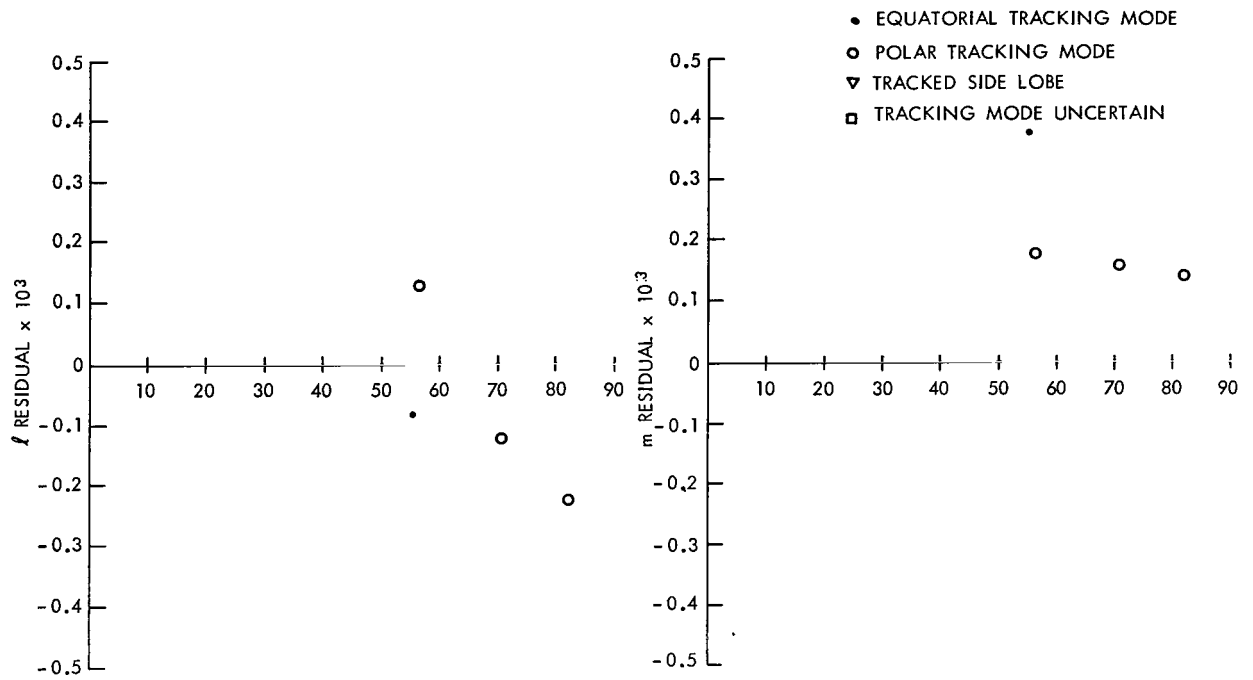


ELEVATION VS DIRECTION COSINE RESIDUAL $\times 10^3$
 g. Winkfield, England 15 observations



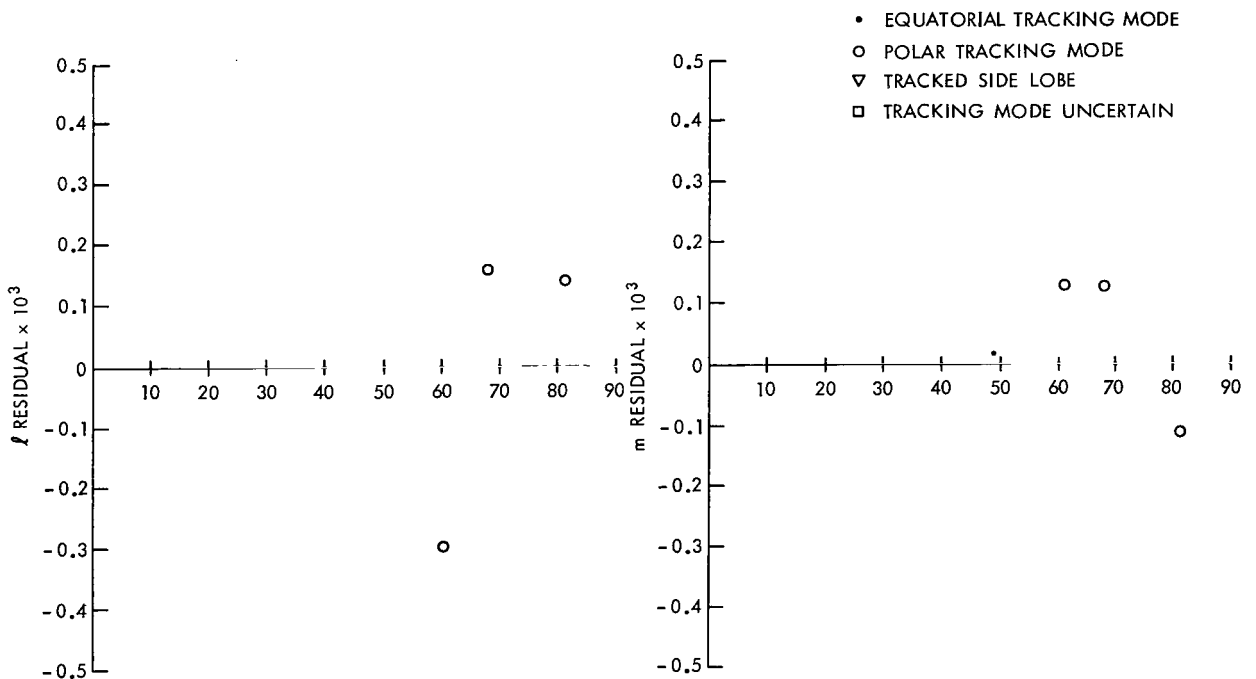
ELEVATION VS DIRECTION COSINE RESIDUAL $\times 10^3$
 h. Lima, Peru 6 observations

Figure 8—Plots of elevation vs direction cosine residuals (elevation vs $\Delta l \times 10^3$ and elevation vs $\Delta m \times 10^3$) and mode of tracking (polar or equatorial).



ELEVATION VS DIRECTION COSINE RESIDUAL $\times 10^3$

i. Quito, Ecuador 4 observations



ELEVATION VS DIRECTION COSINE RESIDUAL 1×10^3

j. Santiago, Chile 4 observations

Figure 8—Plots of elevation vs direction cosine residuals (elevation vs $\Delta l \times 10^3$ and elevation vs $\Delta m \times 10^3$) and mode of tracking (polar or equatorial).

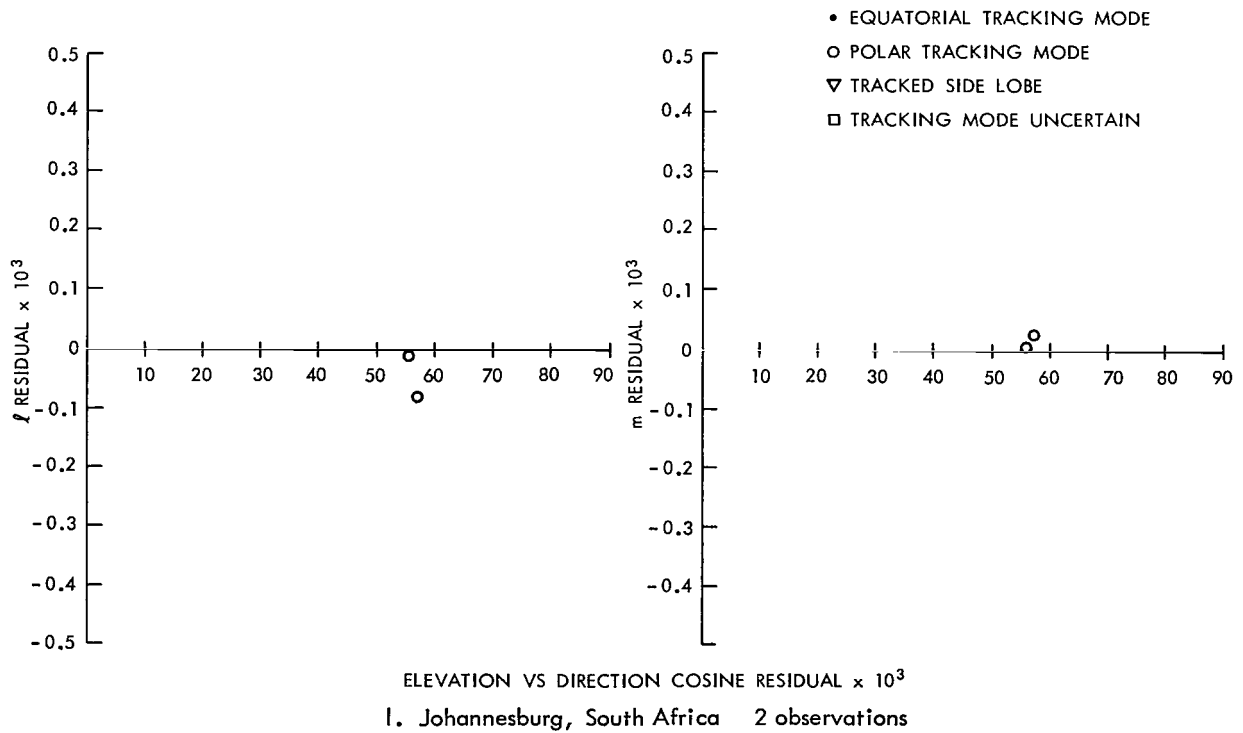
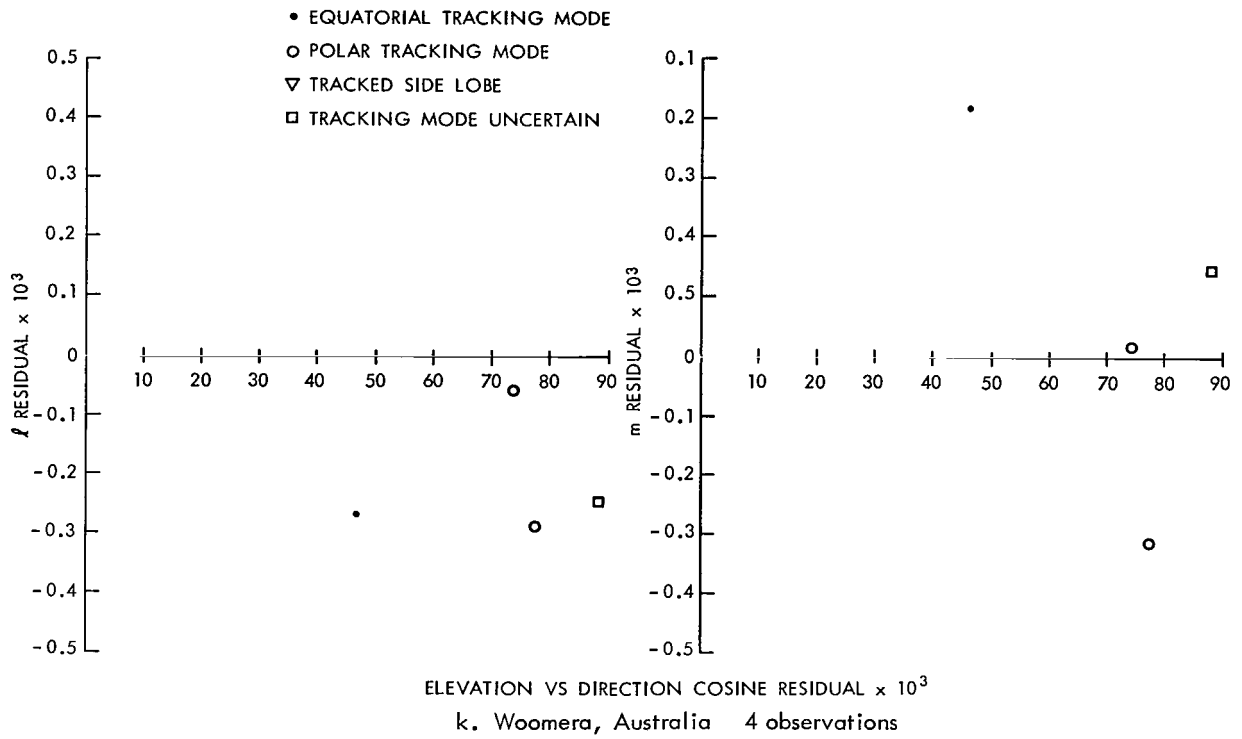


Figure 8—Plots of elevation vs direction cosine residuals (elevation vs $\Delta l \times 10^3$ and elevation vs $\Delta m \times 10^3$) and mode of tracking (polar or equatorial).

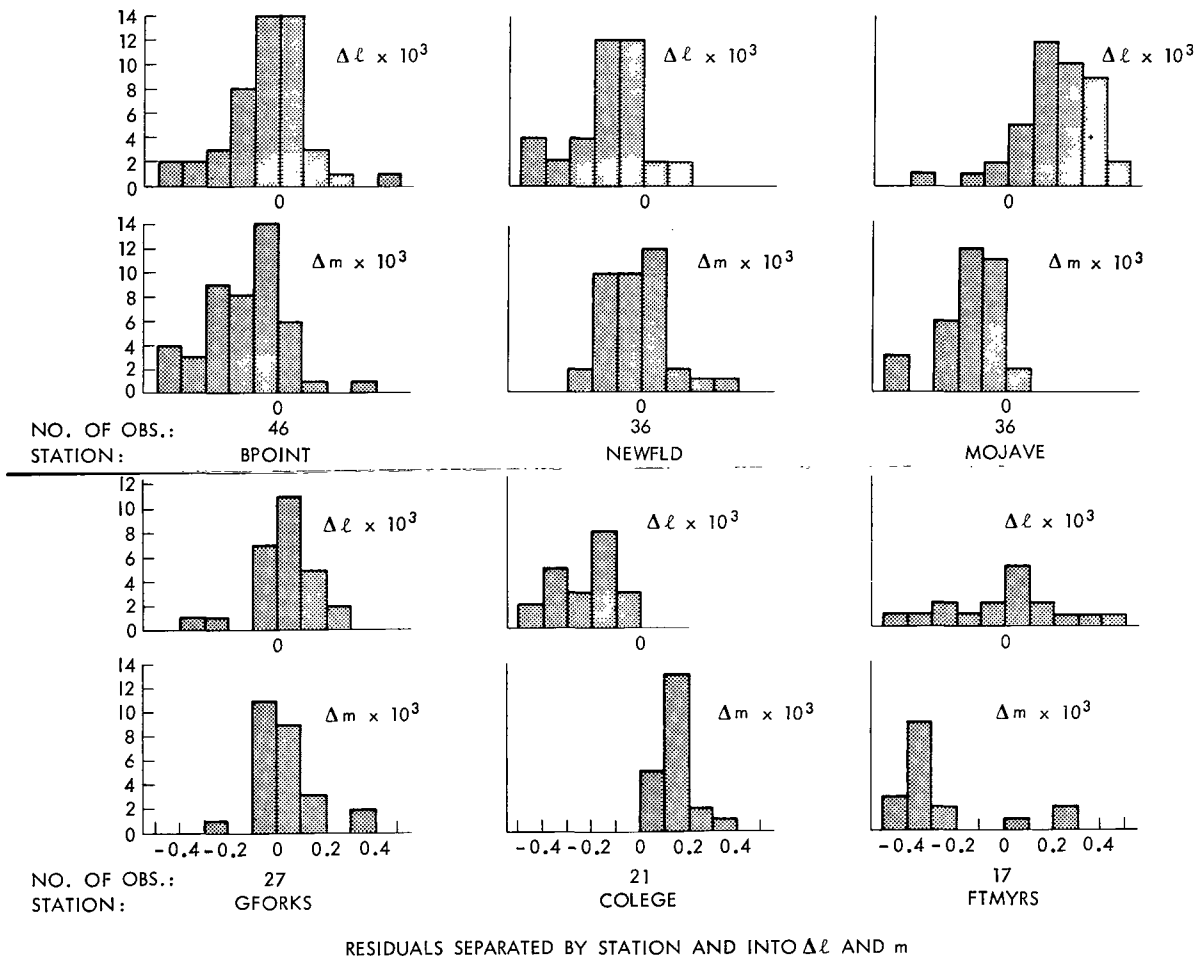


Figure 9a—Histogram of Minitrack residuals calculated from optically-determined "standard orbit"—residuals separated by station and into $\Delta\ell$ and Δm .

To illustrate the possibility of reducing the standard deviation of the data, a sample calculation was made for Mojave (Figures 8b and 9a). Considering $\Delta\ell$ and Δm both separately and together, the following mean values and standard deviations were obtained:

	\bar{x}	σ
$\Delta\ell$ only	$+0.18 \times 10^{-3}$	0.18×10^{-3}
Δm only	-0.16×10^{-3}	0.05×10^{-3}
$\Delta\ell + \Delta m$	$+0.01 \times 10^{-3}$	0.23×10^{-3}

It is seen that the standard deviation of $\Delta\ell$ only is approximately 25 percent smaller than the standard deviation of $\Delta\ell$ and Δm considered together. Next, the assumption was made that the biases for Mojave were known and that their effects caused the mean offsets of $+0.18 \times 10^{-3}$ and -0.16×10^{-3}

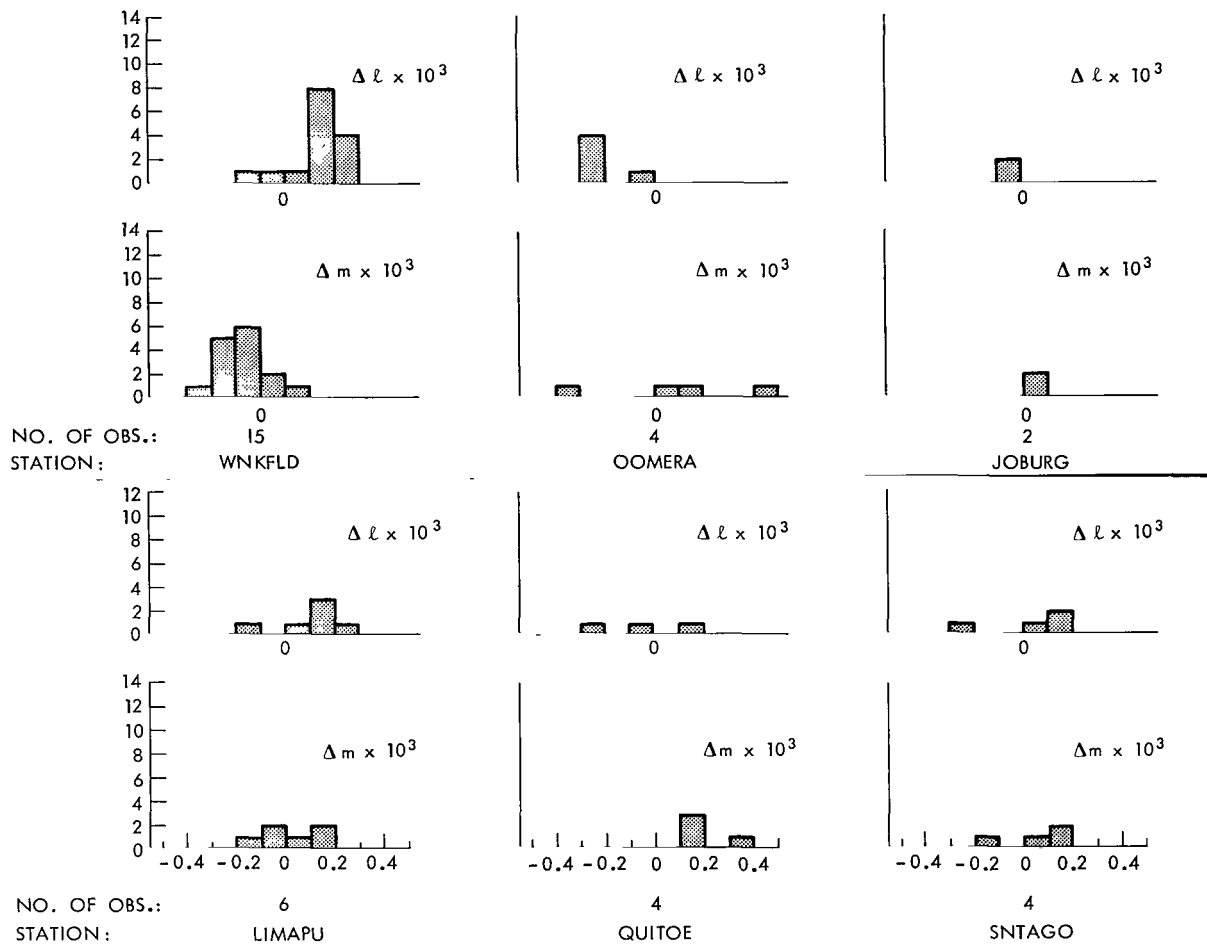


Figure 9b—Histogram of Minitrack residuals calculated from optically-determined "standard orbit"—residuals separated by station and into $\Delta \ell$ and Δm .

respectively in $\Delta \ell$ and Δm . A further assumption was made that the effect of removing known biases could be approximated by subtracting the mean offsets from the corresponding residual sets. The standard deviation of the entire combined data set (ℓ and m together) was then recalculated after the offsets had been subtracted from the original residual set. The new value of the standard deviation was 0.15×10^{-3} compared to the original value of 0.23×10^{-3} , a reduction of approximately 33 percent. Although Mojave represented one of the most biased of the data sets used in this analysis, this simple procedure reduced the standard deviation for Mojave to a value below the overall rms of fit of 0.19×10^{-3} for the entire data set. A further inspection of the Mojave residuals in Figure 8b indicates also that this bias is not primarily due to refraction-dependent residuals as defined earlier, since the Δm_{polar} residuals in Figure 8b show a strong negative bias although they are refraction-independent. Despite the indications of station biases noted in this section, however, it is felt that additional data sets should be examined before any definitive inferences of station biases can be properly made, since the data set analyzed extended for only 5-1/4 days. In a computer program which employs a rejection criterion for the use of data in orbital solutions, these

apparent station biases could cause an unwarranted rejection of data which might be basically good data. For example, it was noted in the fourth section ("Summary of Minitrack Data") that 10 per cent of the data from College, Alaska, had residuals which exceeded 0.5×10^{-3} (the rejection criterion employed for analysis purposes in this paper).

DIFFERENCES IN ORBITS ADJUSTED USING MINITRACK DATA ONLY AND OPTICAL DATA ONLY

In order to obtain an estimate of the actual differences of position in inertial space as obtained by a Minitrack-determined orbit and an optically-determined orbit, trajectories obtained from the two adjusted solutions were calculated, differenced, and resolved into along-track, cross-track, and radial differences. The rms of fit of the orbit adjusted by Minitrack data only, not corrected for refraction or other effects, was 0.19×10^{-3} in terms of direction cosine for the 5-1/4-day arc used in the "standard" orbit solution. The position and velocity vectors for the epoch 01^h 38^m 22^s.000 12/31/1965 UTC, which were adjusted on the basis of the 436 Minitrack observations, are given in Table 6. The Minitrack data included observations down to 15° elevation. The rms of fit of the standard orbit adjusted by optical data only was 3'0. In both this calculation and the previous analysis, the start and end points of the Minitrack data were chosen to correspond to the equivalent start and end times of the optical data so that there would be no systematic orbital shift caused by overlap effects. The along-track, cross-track, and radial position differences of the first and last four hours of the Minitrack and optical orbits are shown in Figure 10. The along-track difference takes the approximate form of a sine curve with a two-hour period (the period of GEOS I) with an amplitude of approximately 110 meters superimposed upon a small secular term. The secular portion of the curve has a rate of approximately 16 meters/day. Considering the optical orbit as an error-free "reference orbit," the root mean square of the total position errors over the 5-1/4-day

Table 6

Final Adjusted Position and Velocity Vectors at
Epoch for the Minitrack-Determined Orbit.

Minitrack-Adjusted Position Vector	Minitrack-Adjusted Velocity Vector
X: +5,690,533.8 meters	\dot{X} : -4,685.6272 meters/sec.
Y: +1,474,657.9 meters	\dot{Y} : +3,849.5020 meters/sec.
Z: +6,013,372.3 meters	\dot{Z} : +2,939.1288 meters/sec.
Epoch:	01 ^h 38 ^m 22 ^s .000 12/31/1965 UTC
No. of Observations:	436
Arc Length:	5-1/4 days
Rms of Fit:	1.906×10^{-4}

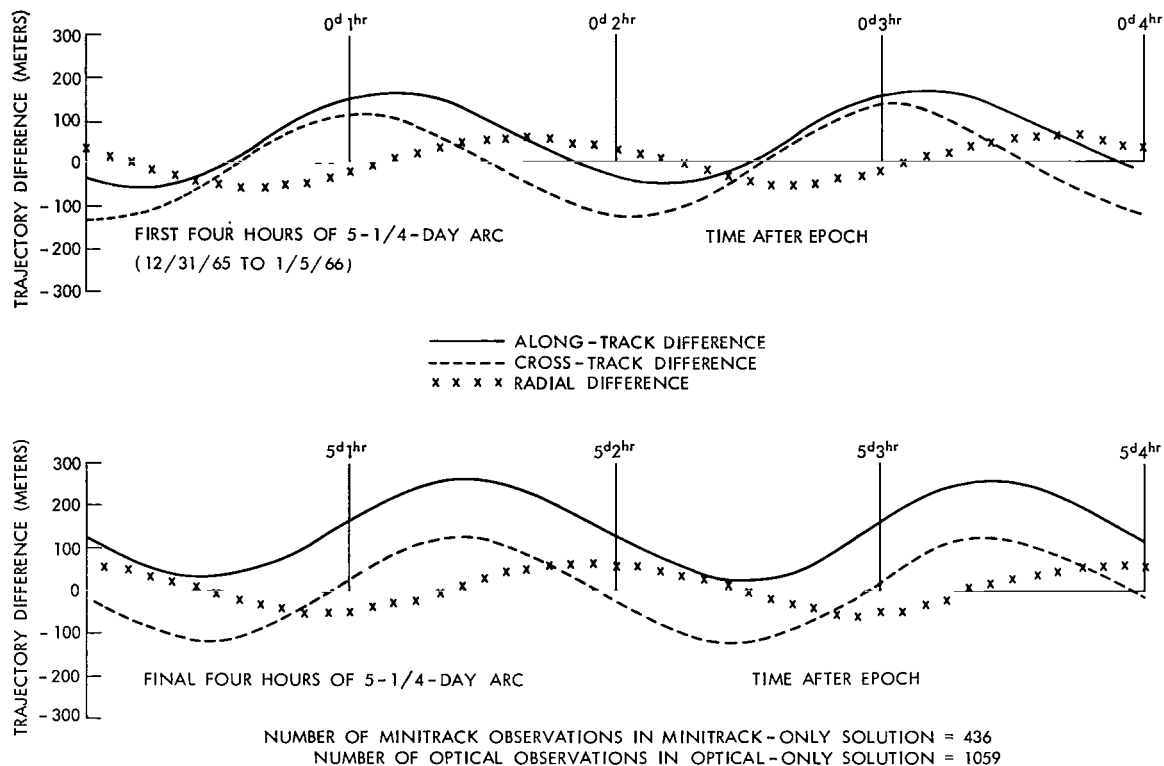


Figure 10—Differences between 5-1/4-day trajectories adjusted by Minitrack data only and optical data only using the SAO M-1 gravity model. (Differences are resolved along-track, cross-track and radially.)

arc of the Minitrack orbit was approximately 165 meters. The Minitrack solution utilized data down to approximately 15° elevation, was not corrected for tropospheric or ionospheric refraction, and was not weighted according to elevation to compensate for any deterioration of the data at the lower elevations.

CONCLUSIONS

It has been shown that an optically-determined orbit is sufficiently accurate for evaluating Minitrack data. The standard deviation of position of the Minitrack-determined orbit analyzed in this report, using an optically-determined orbit as a standard, was approximately 165 meters for a 5-1/4-day arc. The Minitrack-determined orbit used data acquired down to 15° elevation. These data were not corrected for tropospheric or ionospheric refraction and were not weighted in the solution for elevation effects. The comparatively small standard deviation of 165 meters which resulted may be attributed in large part to a careful selection of computing tools used in the analysis. In particular, the use of an extremely accurate gravity model (SAO M-1 model) and a tracking complement referred to a datum consistent with this gravity model (SAO C-5) contributed to the accuracy of the results obtained. (See Reference 16 for a more detailed analysis of gravity



effects.) The relatively small standard deviation also suggests that low-elevation Minitrack data when corrected for refraction effects may possibly be used with confidence in orbital solutions.

The use of optical data as an independent data set revealed systematic offsets of the residuals at certain Minitrack sites. The use of such an independent data set could be effectively used to determine the calibration coefficients for the individual Minitrack stations and to investigate the feasibility of using the Minitrack data for self-calibration purposes.

Goddard Space Flight Center
National Aeronautics and Space Administration
Greenbelt, Maryland, January 6, 1969
311-07-21-01-51

REFERENCES

1. NASA-GSFC Operations Plan 11-65 Geodetic Satellite (GEOS-A), August 1965, NASA-GSFC Document X-513-65-345.
2. Lundquist, C. A., and Veis, G., "Geodetic Parameters for a 1966 Smithsonian Institution Standard Earth," SAO Special Report No. 200, Vol. 1, 1966.
3. Kaula, W. M., "Celestial Geodesy," NASA Technical Note D-1155, March 1962.
4. Köhnlein, W., "The Earth's Gravitational Field as Derived from a Combination of Satellite Data with Gravity Anomalies," prepared for XIV General Assembly, International Union of Geodesy and Geophysics, International Association of Geodesy, October 1967.
5. New Mexico State University, Physical Science Laboratory, "Inspection of the 136.5 MC Minitrack STADAN Antennas at Santiago, Chile, S. A.," January 1965.
6. Aero Geo Astro, "Minitrack Calibration System Model 2, Ground Equipment Instruction Manual."
7. Berbert, J. H., Oosterhout, J. D., Engels, P. D., and Habib, E. J., "Minitrack Calibration System," March-April, 1963, Photographic Science and Engineering, Vol. 7, No. 2.
8. Vonbun, F. O., "Corrections for Atmospheric Refraction at the NASA Minitrack Stations," NASA Technical Note D-1448, August 1962.
9. NASA, "Handbook of Operating Instructions for Minitrack and Telemetry Systems," January 12, 1961.
10. Bendix Corp., "Instruction Manual for 136 MC Minitrack Interferometer System," Vol. I of II.
11. Bendix Radio, "Instruction Book for Minitrack Satellite Tracking Unit Designed by U. S. Naval Research Laboratory (108 MC)."

12. NASA, Project Vanguard, Tracking and Guidance Branch (compilation), "Minitrack System Training Manual (Revised September 1958)."
13. Sapper, Larry W., GSFC, memoranda for record:
 - a. "Reduction of Raw Minitrack Phase Angle Data to Direction Cosines ℓ and m ," November 24, 1965.
 - b. "Addendum to Memorandum for Record: Reduction of Raw Minitrack Phase Angle Data to Direction Cosines ℓ and m ," February 16, 1966.
 - c. "Interpolation of the Medium and Coarse Phase Angles in the Reduction of Minitrack Data," March 1, 1966.
14. Evans, C. H., and Cole, I. J., GSFC, AOPB Systems Manual Program Descriptions:
 - a. "F036—Ionosphere Data Load," November 1965.
 - b. "F037—Ionosphere Data Search," November 1965.
15. Cole, I. J., GSFC, AOPB Systems Manual Program Description, "F116— ℓ , m , ρ , $\dot{\rho}$ Corrector for Ionosphere Refraction," November 1965.

BIBLIOGRAPHY

Cannaday, D. J., GSFC, private communication.

R. H. Gooding, "Orbit Determination from Minitrack Observations."

"GEOS Integrated Investigation Plan," September 23, 1965, prepared for NASA by System Sciences Corporation.

"GEOS-A Mission Plan," September 16, 1965, prepared for NASA by System Sciences Corporation.

"Technical Plan for a National Geodetic Satellite Program," submitted to NASA by the Applied Physics Laboratory, John Hopkins University, Silver Spring, Md., March 1965.

Appendix A

Brief Description of the 136-Mc Minitrack Interferometer Tracking System

The basic Minitrack configuration consists of an antenna field of 13 antennas arranged as shown in Figure A1. In addition to the antenna system, there is an operations building housing the electronic systems. A MOTS 40-inch-focal-length camera is located at the exact center of the fine-beam arrays of the antenna system. This camera is normally used for calibrating the antenna system by photographing an airborne flashing light beacon against a background of stars while the antenna system is simultaneously receiving a 136-Mc radio signal from the same airborne source. Since theoretically the physical location of the MOTS camera and the antenna system center are identical, a unique system is available for intercomparing the two distinct types of tracking systems.

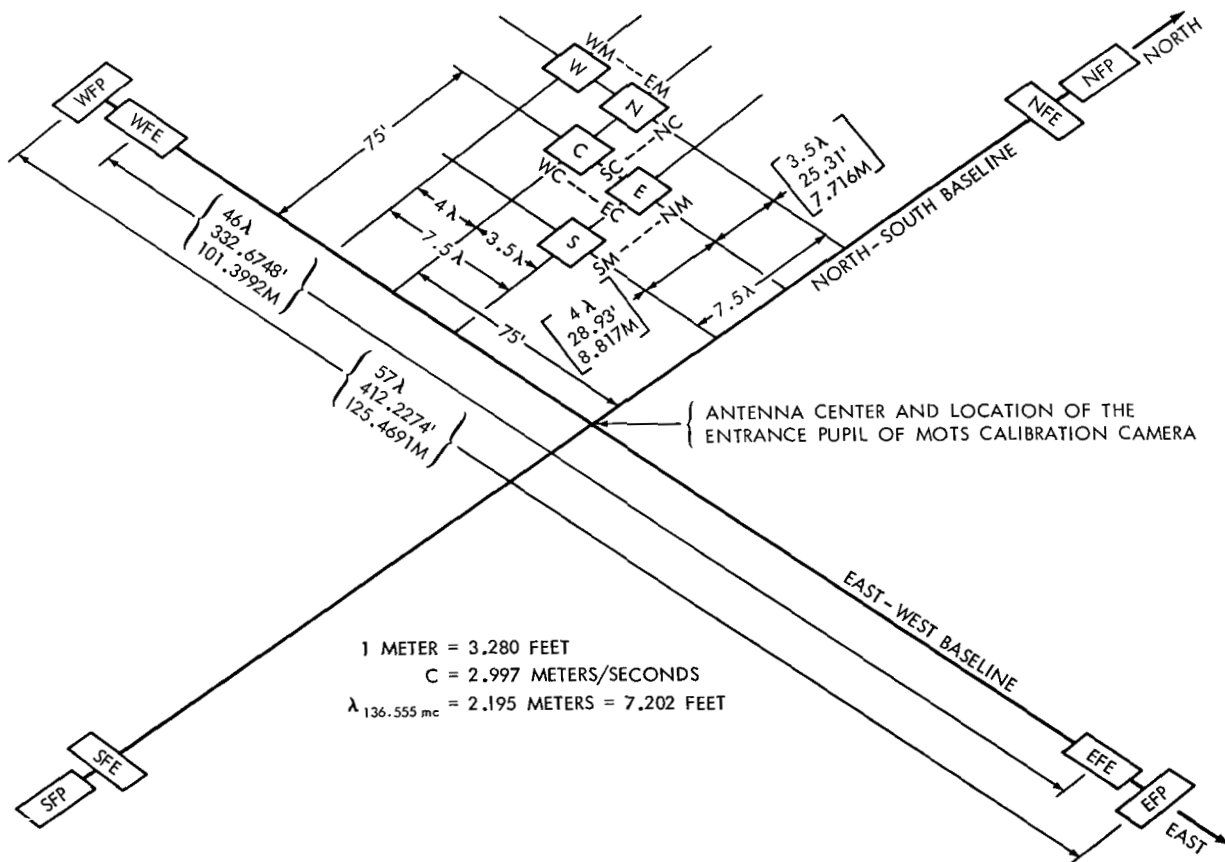


Figure A1—136-Mc Minitrack antenna layout.

The electronics of the Minitrack interferometer system is designed to locate satellites transmitting on 1000 separate frequencies ranging from 136.000 Mc to 136.999 Mc in 1-kc steps. The tracking is performed in a completely passive mode. The possibility of extending this range to 138 Mc is currently being considered.

The antenna system is designed to be highly directive, resulting in a high signal gain. There are two possible modes of tracking, the "equatorial" mode and the "polar" mode. The wavelength dimensions displayed in Figure A1 are based upon a received signal whose frequency is 136.555 Mc.

The antenna arrays located at the ends of the north-south and east-west baselines are used in sets of four for each of the two tracking modes and are abbreviated as follows:

Group 1 — Equatorial Tracking Mode

Equatorial Fine-Beam Arrays

NFE North Fine Equatorial

SFE South Fine Equatorial

EFE East Fine Equatorial

WFE West Fine Equatorial

Group 2 — Polar Tracking Mode

Polar Fine-Beam Arrays

NFP North Fine Polar

SFP South Fine Polar

AFP East Fine Polar

WFP West Fine Polar

The distance between NFE and SFE is the same as indicated between EFE and WFE. Also, the distance between NFP and SFP is the same as indicated between AFP and WFP.

The reception pattern of Group 1 (Equatorial Fine-Beam) is shown on the left side of Figure A2. The reception pattern of Group 2 (Polar Fine-Beam) is shown on the right side of the same figure. These two groups comprise the accurate portion of the antenna system. The individual stations can electronically switch between the polar and equatorial modes of tracking very quickly, so that both modes of tracking are possible on the same pass of a satellite. The actual shape of the wedge or fan-shaped pattern of the fine beam is defined by the locus of points where the signal from the satellite's Minitrack beacon drops 3 decibels from the zenith signal. Under normal conditions, the satellite is tracked only when it is located with this wedge-shaped fine beam. Tracking is usually further restricted to a maximum distance of 20° each way from the zenith in the long-beam direction

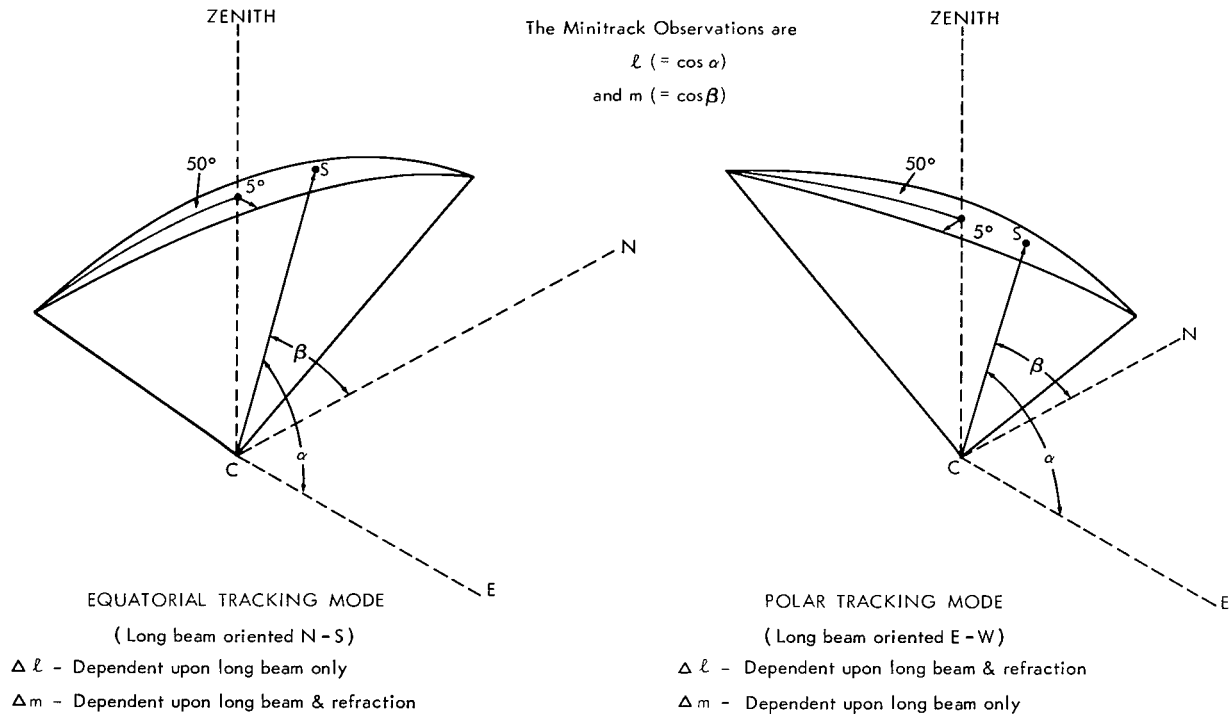


Figure A2—Approximate reception pattern of the fine beam of the 136-Mc Minitrack antenna array.

of this pattern in order to minimize refraction effects. A typical reception pattern for the EFE array in the east-west direction at the Minitrack station at Santiago, Chile, is shown in Figure A3.

In order to calculate the direction cosines of a satellite, it is necessary to know the absolute phase difference of the signal as received simultaneously by a pair of the fine-beam antennas, for example, WFE and EFE. Since only relative phase differences of the signal can be measured as received by the fine-beam pairs, it is necessary to introduce

five additional arrays to resolve these phase-difference ambiguities which arise. The ambiguity antennas are labeled in Figure A1 as W, N, C, E, S (West, North, Common, East, and South respectively). This group of five antennas can be used to resolve the ambiguities for both the Group 1 and Group 2 fine-beam arrays. The W-N and E-S combinations are used for east-west medium and north-south medium resolution respectively. The N-C and C-E combinations are used for north-south and east-west coarse resolution respectively. In being so used, the combinations are separated by 4 and 3.5 wavelengths respectively, so that the difference in separation of the medium

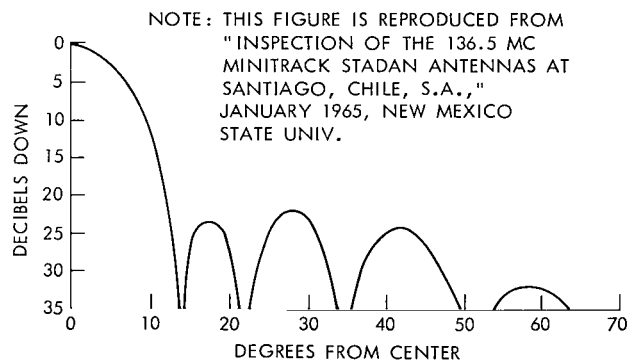
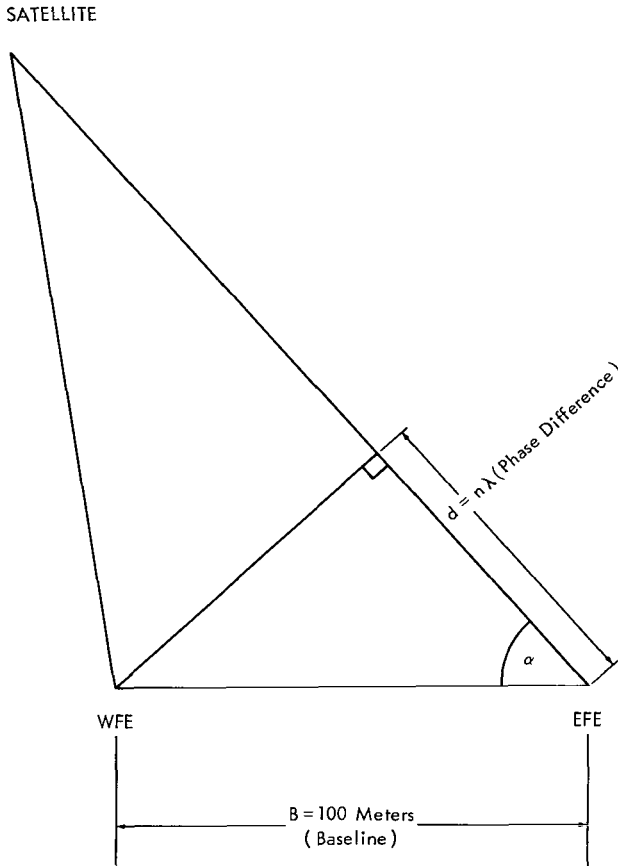


Figure A3—Antenna pattern for east fine equatorial Minitrack antenna at Santiago, Chile.

and coarse combinations used to resolve either north-south or east-west ambiguities is only 1/2 of a wavelength.

The electronics of the Minitrack system divides the 360 electrical degrees phase measurement into 1000 parts of 0.36 electrical degrees each. This measurement represents the upper precision limit of the equipment. If it is assumed that the fine-beam baseline is approximately 100 meters (see Figure A4), the resulting accuracy in terms of space angle can be estimated approximately by the following procedure. The direction cosine ℓ (considering the east-west baseline) is related to the electrical phase angle by the equation



$$\ell = \cos \alpha = \frac{d}{B} = \frac{n\lambda}{B}$$

$$= \frac{\phi}{2\pi} \frac{\lambda}{B},$$

where

ϕ = electrical angle in radians,

λ = signal wavelength,

\cong 2.2 meters at 136.555 Mc,

B = antenna separation distance or baseline length,

\cong 100 meters,

d = phase difference in linear measure,

n = phase difference in number of wavelengths of signal.

Figure A4—Simplified geometry of satellite 136-Mc Minitrack beacon signal as received by the west fine equatorial and east fine equatorial antenna arrays.

If ϕ is measured in degrees, the equation becomes

$$\ell = \cos \alpha = \frac{\phi}{360^\circ} \frac{2.2}{100}.$$

To find the error in ℓ and α ,

$$\Delta \ell = -\sin \alpha \Delta \alpha = \frac{2.2}{360 \times 100} \Delta \phi$$

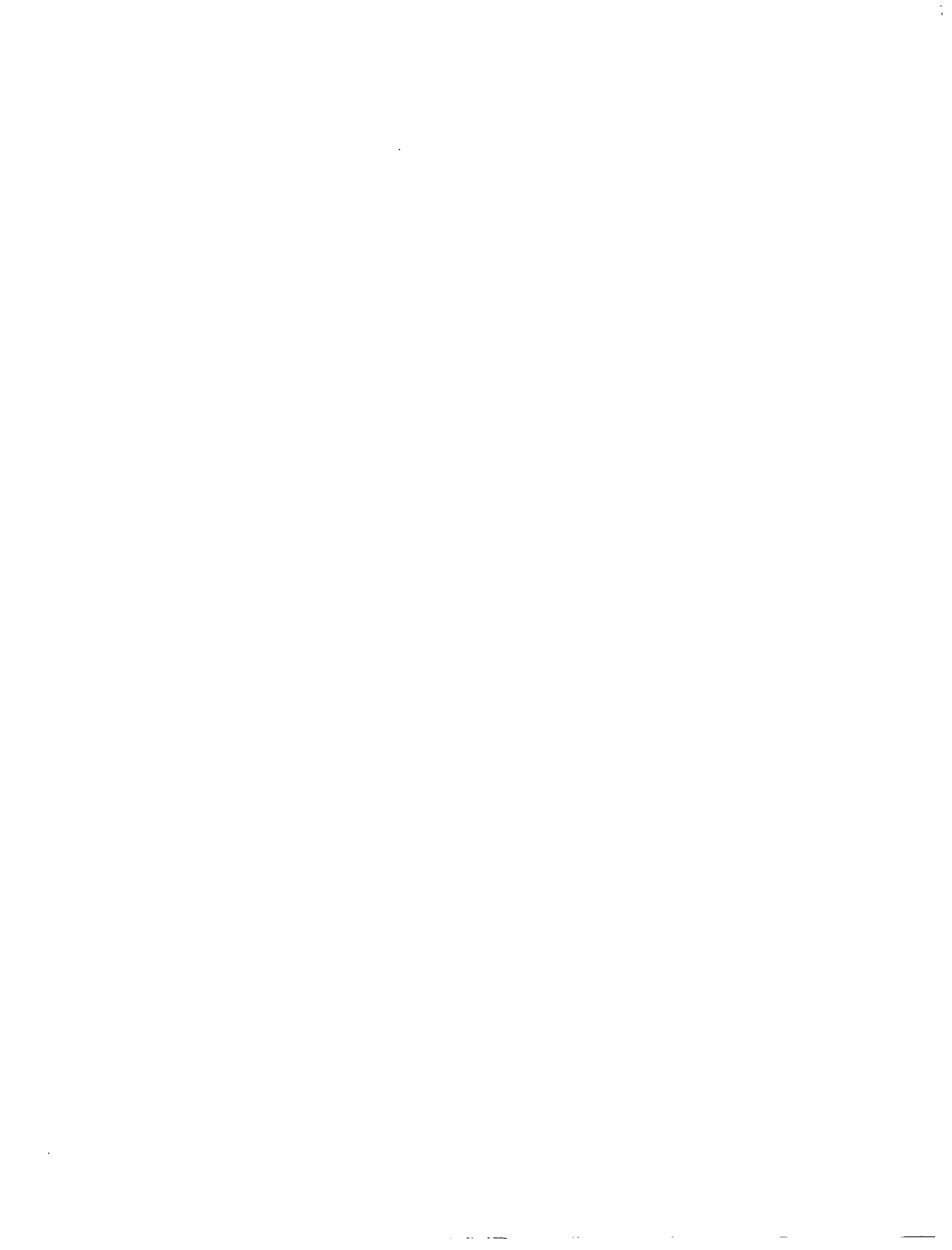
$$= \frac{2.2}{3.6} \times 10^{-4} \Delta \phi.$$

If $\Delta\phi = 0.36$ degrees, then

$$\begin{aligned}\Delta\ell &= -\sin\alpha\Delta\alpha = \frac{2.2}{3.6} \times 0.36 \times 10^{-4} \\ &= 2.2 \times 10^{-5} .\end{aligned}$$

For a near-overhead pass, $\sin\alpha \simeq 1$. Neglecting the minus sign,

$$\begin{aligned}\Delta\alpha &= 2.2 \times 10^{-5} \text{ radians} \\ &= 2.2 \times 10^{-5} \times (2 \times 10^5)'' \\ &= 4.4 .\end{aligned}$$



Appendix B

Preprocessing of Optical Observations

Preprocessing of Optical Data

The first step in the processing of optical observations (and one usually performed by the observing source) consists of developing a plate or film and identifying thereon the image or images of the satellite and the images of several reference stars whose right ascensions and declinations are well known. The initial measurements both of satellite images and of reference stars consist of linear rectangular coordinates. From the knowledge of the spherical coordinates of the reference stars, the right ascensions and declinations of the satellite images may be calculated. These coordinates as received by the preprocessor may be referred to the mean equator and equinox of date, true equator and equinox of date, or mean equator and equinox of some standard epoch.

The preprocessor then transforms these observations to a common coordinate system. It transforms all right ascensions and declinations to the true equator and equinox of the epoch of the observations being processed. If the observations were originally referred to the mean equator and equinox of a particular epoch, it is necessary only to precess from that epoch to the epoch of the observations. However, if they were referred to the true equator and equinox of a particular epoch, it is necessary first to transform them to the mean equator and equinox of that same epoch and then precess to the epoch of the observations. Finally, a transformation must be made from the mean equator and equinox of the epoch of the observations to the true equator and equinox of the epoch of the observations.

Nutation

The transformation from the true equator and equinox of date to the mean equator and equinox of date is

$$Y = NX ,$$

where

$$Y = \begin{bmatrix} \cos \delta_m & \cos a_m \\ \cos \delta_m & \sin a_m \\ \sin \delta_m & \end{bmatrix} ,$$
$$X = \begin{bmatrix} \cos \delta_T & \cos a_T \\ \cos \delta_T & \sin a_T \\ \sin \delta_T & \end{bmatrix} ,$$

$$N = \begin{bmatrix} 1 & \Delta\psi \cos \epsilon_m & \Delta\psi \sin \epsilon_m \\ -\Delta\psi \cos \epsilon_m & 1 & \Delta\epsilon \\ -\Delta\psi \sin \epsilon_m & -\Delta\epsilon & 1 \end{bmatrix},$$

and

α_m, δ_m = right ascension and declination referred to mean equator and equinox of date,

α_T, δ_T = right ascension and declination referred to true equator and equinox of date,

ϵ_m = mean obliquity of date,

$\Delta\psi$ = nutation in longitude, and

$\Delta\epsilon$ = nutation in obliquity.

The inverse transformation is simply:

$$X = N^{-1} Y = N^T Y.$$

Precession

The transformation from the mean equator and equinox of 1950.0 to the mean equator and equinox of an arbitrary epoch t_1 is

$$Y = PX,$$

where

$$Y = \begin{bmatrix} \cos \delta_{t_1} & \cos \alpha_{t_1} \\ \cos \delta_{t_1} & \sin \alpha_{t_1} \\ \sin \delta_{t_1} & \end{bmatrix},$$

$$X = \begin{bmatrix} \cos \delta_{1950.0} & \cos \alpha_{1950.0} \\ \cos \delta_{1950.0} & \sin \alpha_{1950.0} \\ \sin \delta_{1950.0} & \end{bmatrix},$$

and

$$P = \begin{bmatrix} (\cos z \cos \theta \cos \zeta - \sin z \sin \zeta) & (-\cos z \cos \theta \sin \zeta - \sin z \cos \zeta) & (-\cos z \sin \theta) \\ (\sin z \cos \theta \cos \zeta + \cos z \sin \zeta) & (-\sin z \cos \theta \sin \zeta + \cos z \cos \zeta) & (-\sin z \sin \theta) \\ (\sin \theta \cos \zeta) & (-\sin \theta \sin \zeta) & (\cos \theta) \end{bmatrix}.$$

The inverse transformation is

$$X = P^{-1}Y = P^T Y .$$

Since the expressions in z , θ , ζ are tied to 1950.0 as an epoch, the precession between two different epochs, neither of which is 1950.0, must be performed in two steps, using 1950.0 as an intermediary epoch. The above expression for P is rigorous. There are simple third-degree polynomials in time derived by Newcomb which permit the calculation of z , θ , and ζ . There exists an even simpler form of the matrix P which permits the calculation of its elements by means of third-degree polynomials expressed directly in terms of the variable t (time). This simplification bypasses the necessity of calculating the sines and cosines of the angles z , θ , and ζ . These simplified matrix elements are derived by expanding the sines and cosines of z , θ , and ζ , contained in the elements of P , into a series, performing the necessary multiplications, and dropping terms exceeding the third degree. The appropriate polynomial expressions in t are then substituted into the remaining expressions containing z , θ , and ζ . After the necessary multiplications have again been performed, all terms in t higher than the third degree are dropped. The final expression for P then consists simply of nine elements in terms of a third-degree polynomial in time.



Appendix C

Force Models Used in NONAME

Force Models

The data reduction program in its present form incorporates four force models. These are:

1. The earth's gravitational field;
2. The solar and lunar gravitational perturbations;
3. Solar radiation pressure;
4. Atmospheric drag.

The program is so designed that the gravitational coefficients and pertinent physical characteristics of satellites, such as reflectivity, cross-sectional area mass, and drag coefficient, can be simply changed through card input or block data statement.

The Earth's Gravitational Field

The formulation of the geopotential used is:

$$u = \frac{GM}{r} \left\{ 1 + \sum_{n=2}^k \sum_{m=0}^n \left(\frac{a}{r} \right)^n P_n^m(\sin \phi) [C_{nm} \cos m\lambda + S_{nm} \sin m\lambda] \right\}, \quad (C1)$$

where

G is the universal gravitational constant,

M is the mass of the earth,

r is the geocentric distance to the satellite

a is the earth's mean equatorial radius,

ϕ is the sub-satellite latitude,

λ is the sub-satellite east longitude, and

$P_n^m(\sin \phi)$ is the associated spherical harmonic of degree n and order m .

The design of the potential function requires that normalized gravitational coefficients $C_{n,m}$ and $S_{n,m}$ be used. The program is presently capable of accepting coefficients up to (20, 20) or any subset of these.

The SAO M-1 earth gravitational model (Reference C1) modified by the GEOS I resonant harmonics ($\bar{C}_{13,12}$, $\bar{S}_{13,12}$, $\bar{C}_{14,12}$, $\bar{S}_{14,12}$, $\bar{C}_{15,12}$, $\bar{S}_{15,12}$) (Reference C2) is listed in Table C1. These

Table C1

SAO M-1 Harmonic Coefficients (Normalized).

n	m	$\bar{C} \times 10^6$	$\bar{S} \times 10^6$	n	m	$\bar{C} \times 10^6$	$\bar{S} \times 10^6$
2	0	-484.1735		8	2	0.026	0.039
2	1			8	3	-0.037	0.004
2	2	2.379	-1.351	8	4	-0.212	-0.012
				8	5	-0.053	0.118
3	0	0.9623		8	6	-0.017	0.318
3	1	1.936	0.266	8	7	-0.0087	0.031
3	2	0.734	-0.538	8	8	-0.248	0.102
3	3	0.561	1.620				
				9	0	0.0122	
4	0	0.5497		9	1	0.117	0.012
4	1	-0.572	-0.469	9	2	-0.0040	0.035
4	2	0.330	0.661				
4	3	0.851	-0.190	10	00	0.0118	
4	4	-0.053	0.230	10	01	0.105	-0.126
				10	02	-0.105	-0.042
5	0	0.0633		10	03	-0.065	0.030
5	1	-0.079	-0.103	10	04	-0.074	-0.111
5	2	0.631	-0.232				
5	3	-0.520	0.007	11	00	-0.0630	
5	4	-0.265	0.064	11	01	-0.053	0.015
5	5	0.156	-0.592				
				12	00	0.0714	
6	0	-0.1792		12	01	-0.163	-0.071
6	1	-0.047	-0.027	12	02	-0.103	-0.0051
6	2	0.069	-0.366	12	12	-0.031	0.0008
6	3	-0.054	0.031	13	00	0.0219	
6	4	-0.044	-0.518	13	12	-0.06769	0.06245
6	5	-0.313	-0.458	13	13	-0.059	0.077
6	6	-0.040	-0.155				
				14	00	-0.0332	
7	0	0.0860		14	01	-0.015	0.0053
7	1	0.197	0.156	14	11	0.0002	-0.0001
7	2	0.364	0.163	14	12	0.00261	-0.02457
7	3	0.250	0.018	14	14	-0.014	-0.003
7	4	-0.152	-0.102				
7	5	0.076	0.054	15	09	-0.0009	-0.0018
7	6	-0.209	0.063	15	12	-0.07473	-0.01026
7	7	0.055	0.096	15	13	-0.058	-0.046
8	0	0.0655		15	14	0.0043	-0.0211
8	1	-0.075	0.065				

The normalized coefficients ($\bar{C}_{n,m}$, $\bar{S}_{n,m}$) are related to the denormalized coefficients ($C_{n,m}$, $S_{n,m}$) as indicated below:

$$C_{(n,m)} = \left[\frac{(n-m)! (2n+1)k}{(n+m)!} \right]^{1/2} \bar{C}_{(n,m)}$$

$$S_{(n,m)} = \left[\frac{(n-m)! (2n+1)k}{(n+m)!} \right]^{1/2} \bar{S}_{(n,m)}$$

$$k = 1 \text{ when } m = 0$$

$$k = 2 \text{ when } m \neq 0$$

coefficients have been used extensively in the NONAME orbit determination program for the reduction of GEOS I optical and electronic data. The same data sets have been reduced using various other gravity models. An intercomparison of the results can be found in Reference C3.

The transformation of the geopotential in earth-fixed coordinates (r, ϕ, λ) to gravitational accelerations in inertial coordinates (x, y, z) is accomplished as follows:

$$\ddot{x}_{\oplus} = \frac{\partial u}{\partial r} \frac{\partial r}{\partial x} + \frac{\partial u}{\partial \phi} \frac{\partial \phi}{\partial x} + \frac{\partial u}{\partial \lambda} \frac{\partial \lambda}{\partial x}; \quad (C2)$$

and similarly for \ddot{y}_{\oplus} , \ddot{z}_{\oplus} , where the subscript " \oplus " denotes accelerations caused by the earth's field.

Solar and Lunar Gravitational Perturbations

The perturbations caused by a third body, e.g., the sun or moon, on a satellite orbit are treated by defining a disturbing function R (Reference C4) which can be treated as the potential function U . The solar perturbation R_{\odot} takes the form

$$R_{\odot} = \frac{GMm_{\odot}}{r_{\odot}} \left[\left(1 - \frac{2r}{r_{\odot}} S + \frac{r^2}{r_{\odot}^2} \right)^{-1/2} - \frac{rS}{r_{\odot}} \right], \quad (C3)$$

where

$$S = \cos(\vec{r}, \vec{r}_{\odot})$$

and

m_{\odot} is the mass of the sun in earth masses,

\vec{r}_{\odot} is the geocentric position vector of the sun,

r_{\odot} is the geocentric distance to the sun,

\vec{r} is the geocentric position vector of the satellite,

r is the geocentric distance to the satellite,

G is the universal gravitational constant, and

M is the mass of the earth.

The satellite acceleration due to the sun is then

$$\ddot{x}_{\odot} = \frac{\partial R_{\odot}}{\partial r} \frac{\partial r}{\partial x} + \frac{\partial R_{\odot}}{\partial \phi} \frac{\partial \phi}{\partial x} + \frac{\partial R_{\odot}}{\partial \lambda} \frac{\partial \lambda}{\partial x}; \quad (C4)$$

plus \ddot{y}_{\odot} , \ddot{z}_{\odot} , similarly derived, where λ and ϕ are the longitude and latitude of the satellite respectively. The lunar perturbation is found from Equation C3 by substituting the lunar mass and distance for those of the sun.

The lunar and solar ephemerides are computed internal to the program. These positions are computed at 10 equal intervals over each five-day period and least squares fit to a fourth-order polynomial in time about the midpoint of the five-day period. The positions of these bodies are then determined at each data point by evaluating the polynomial at the observation time.

Solar Radiation Pressure

The satellite acceleration due to solar radiation pressure is formulated as follows (Reference C5):

$$\ddot{x}_{\text{RAD}} = - \frac{AP_{\odot}}{m} \gamma \nu L_x ; \quad (\text{C5})$$

plus \ddot{y}_{RAD} , \ddot{z}_{RAD} , similarly derived, where

\hat{L} is the inertial unit vector from the geocenter to the sun and has the components L_x , L_y , L_z ,

A is the cross-sectional area of the satellite,

m is the satellite mass,

γ is a factor depending on the reflective characteristics of the satellite,

ν is the eclipse factor such that:

$$\nu = \begin{cases} 0 & \text{when satellite is in earth's shadow} \\ 1 & \text{when satellite is illuminated by the sun, and} \end{cases}$$

P_{\odot} is the solar radiation pressure in the vicinity of the earth,

$$4.5 \times 10^{-6} \frac{\text{Newton}}{\text{m}^2} .$$

At present, it is assumed that the satellite is specularly reflecting with reflectivity ρ , and thus

$$\gamma = (1 + \rho) . \quad (\text{C6})$$

The vector \hat{L} and the eclipse factor ν are determined from the solar ephemeris subroutine previously described, and from the satellite ephemeris, and are based upon the approximation of a cylindrical earth shadow.

Atmospheric Drag

The atmospheric decelerations are computed as follows:

$$\ddot{x}_{\text{DRAG}} = - \frac{\rho C_D A v v_x}{2m} ; \quad (\text{C7})$$

plus \ddot{y}_{DRAG} , \ddot{z}_{DRAG} , similarly derived, where

ρ is the ambient atmospheric density,

C_D is the satellite drag coefficient,

A is the projected area of the satellite on a plane perpendicular to direction of motion,

m is the satellite mass.

The velocity vector \vec{v} , given in inertial coordinates by

$$\vec{v} = v_x \hat{i} + v_y \hat{j} + v_z \hat{k} , \quad (\text{C8})$$

can be chosen to be either the velocity relative to the atmosphere, which implies that the atmosphere rotates with the earth, or the inertial velocity, which assumes that the atmosphere is static. Presently, the former assumption is made.

The density ρ is computed from the 1962 U. S. Standard Atmosphere.

REFERENCES

1. Lundquist, C. A., and Veis, G., "Geodetic Parameters for a 1966 Smithsonian Institution Standard Earth," SAO Special Report No. 200, Vol. 1, 1966.
2. Köhnlein, W., "The Earth's Gravitational Field as Derived from a Combination of Satellite Data with Gravity Anomalies," prepared for XIV General Assembly, International Union of Geodesy and Geophysics, International Association of Geodesy, October 1967.
3. Lerch, F. J., Marsh, J. G., and O'Neill, B., "Gravity Model Comparison Using GEOS I Long-Arc Orbital Solutions," NASA Technical Note D-5035, August 1968.
4. Kozai, Y., Smithsonian Astrophysical Observatory Special Report No. 22, "The Earth's Gravitational Potential Derived from the Motion of Satellite 1958 Beta Two," pp. 7-10, 1959.
5. Koelle, H., "Handbook of Astronautical Engineering," New York: McGraw-Hill, 1961, pp. 8-33.



Appendix D

Tracking Station Coordinates

Datum Parameters and Station Coordinates

For the purpose of long-arc satellite data reduction and intercomparison, all GEOS I participating tracking stations have been transformed to a common datum. The common datum selected is the SAO Standard Earth C-5 model (semi-major axis = 6378165 meters, flattening coefficient = 298.25) (Reference D1) in which the Baker-Nunn stations are used as the controlling stations for all other stations to be transformed. Descriptions and formulations to effect the transformations from major and isolated datums are presented in Reference D2. The transformation of local datum station coordinates to a common "center-of-mass reference" system is important to accomplish, since the datum shifts are quite large. For example, on the North American Datum the center-of-mass shift to the C-5 Standard Earth is approximately 250 meters. The center-of-mass coordinates of the SAO C-5 Baker-Nunn stations are assessed by SAO to have approximately 20-meter accuracy.

In order to effect any transformation, the parameters of the original datums must be known as well as the geodetic latitude, longitude, and height. Table D1 provides a listing of the original datums and their parameters on which the stations were originally surveyed. Tables D2 through D11 list alternately the original surveyed ellipsoidal positions and the SAO C-5 ellipsoidal positions for over 100 GEOS I tracking stations that have been used in the long-arc intercomparison effort. These tables contain symbols designating the source of original coordinates. The symbols are defined in the following section, with a list of sources. The C-5 positions for 1TANAN and MADGAR (Reference D3) have been derived by the station estimation technique contained in the Orbit Determination Program NONAME. Tables D12 through D21 provide a listing of the station names from which the six-letter designations have been derived.

Sources

The following sources were used to obtain the original datum positions:

<u>Symbol</u>	<u>Source</u>
A	Geodetic Parameters for a 1966 Smithsonian Institution Standard Earth (Reference D1).
B	Goddard Directory of Tracking Station Locations; August 1966; Goddard Space Flight Center.
C	NWL-8 Geodetic Parameters Based on Doppler Satellite Observations; July 1967; R. Anderle and S. Smith, Naval Weapons Laboratory.

Since the above official documents did not contain all those positions that were to be transformed, it was necessary to contact other sources for the positions of the remaining stations. These sources are:

<u>Symbol</u>	<u>Source</u>
D	Private communication with personnel at SAO (K. Haramundanis, B. Miller, A. Girnius).
E	Private communication with 1381st Geodetic Survey Squadron, USAF (S. Tischler).
F	Private communication with personnel at USC&GS (B. Stevens).
G	Private communication with personnel at U. S. Army Engineers Topographic Laboratories (L. Gambino).
H	Private communication with NASA Space Science Data Center (J. Johns, D. Tidwell).
I	General Station Data Sheet—GEOS A Project Manager, NASA Headquarters.

Table D1

Parameters of Original Datums.

Datum Name	Semi-Major Axis (meters)	1/f
North American (N.A.)	6378206.4	294.9787
European	6378388.0	297.0
Tokyo	6377397.2	299.1528
Argentina	6378388.0	297.0
Mercury	6378166.0	298.3
Madagascar	6378388.0	297.0
Australian Nat'l.	6378160.0	298.25
Old Hawaiian	6378206.4	294.9787
Indian	6377276.3	300.8017
Arc (Cape)	6378249.1	293.4663
1966 Canton ASTRO	6378388.0	297.0
Johnston Island 1961	6378388.0	297.0
Midway ASTRO 1961	6378388.0	297.0
Navy IBEN ASTRO 1947	6378206.4	294.9787
Provisional DOS ASTRO 1962, 65	6378388.0	297.0
Allen Sodano Lt.	6378388.0	297.0
1966 SECOR ASTRO	6378388.0	297.0
Viti Levu 1916	6378249.1	293.4663
Corrego Alegre	6378206.4	294.9787
USGS 1962 ASTRO	6378206.4	294.9787
Berne	6377397.2	299.1528

Table D2
SAO—Optical—Source A.

Source	Name	Station No.	Latitude	Longitude	Geodetic Height (meters)	Datum
	1ORGAN	9001	32°25'24.56 32 25 24.70	253°26'51.17 253 26 48.29	1649 1610	N.A. C-5
	1OLFAN	9002	-25 57 33.85 -25 57 37.67	28 14 53.91 28 14 51.45	1562 1560	Arc (Cape) C-5
	WOOMER	9003	-31 06 07.26 -31 06 04.14	136 46 58.70 136 47 01.93	162 158	Australian C-5
	1SPAIN	9004	36 27 51.24 36 27 46.68	353 47 41.47 353 47 36.55	7 56	European C-5
	1TOKYO	9005	35 40 11.08 35 40 23.03	139 32 28.22 139 32 16.42	58 84	Tokyo C-5
	1NATOL	9006	29 21 38.90 29 21 34.38	79 27 25.61 79 27 27.05	1847 1855	European C-5
	1QUIPA	9007	-16 28 05.09 -16 27 58.04	288 30 22.84 288 30 24.02	2600 2479	N.A. C-5
	1SHRAZ	9008	29 38 17.90 29 38 13.59	52 31 11.80 52 31 11.20	1578 1561	European C-5
	1CURAC	9009	12 05 21.55 12 05 24.93	291 09 42.55 291 09 43.97	23 -33	N.A. C-5
	1JUPTR	9010	27 01 13.00 27 01 14.23	279 53 12.92 279 53 12.95	26 -36	N.A. C-5
	1VILDO	9011	-31 56 36.53 -31 56 36.35	294 53 39.82 294 53 36.11	598 636	Argentinean C-5
	1MAUIO	9012	20 42 37.49 20 42 25.66	203 44 24.11 203 44 33.23	3027 3027	Old Hawaiian C-5
	AUSBAK	9023	-31 23 30.82 -31 23 27.69	136 52 39.02 136 52 42.23	141 137	Australian C-5
	OSLONR	9426	60 12 40.38 60 12 38.88	10 45 08.74 10 45 02.26	585 573	European C-5
I	NATALB*	9029	-05 55 50.00 -05 55 43.49	324 50 18.00 324 50 21.30	112 45	N.A. C-5
D	AGASSI*	9050	42 30 20.97 42 30 20.51	288 26 28.71 288 26 29.79	193 138	N.A. C-5
I	COLDLK*	9424	54 44 38.02 54 44 37.26	249 57 25.85 249 57 21.90	597 548	N.A. C-5
I	EDWAFB*	9425	34 57 50.68 34 57 50.17	242 05 11.39 242 05 07.80	784 754	N.A. C-5
I	RIGLAT*	9428	56 56 54.00 56 56 52.37	24 03 42.00 24 03 37.49	5 -15	European C-5
I	POTDAM*	9429	52 22 55.00 52 22 52.33	13 04 01.00 13 03 55.80	111 106	European C-5
I	ZVENIG*	9430	55 41 37.70 55 41 36.17	36 46 03.00 36 46 00.17	145 114	European C-5

*These SAO station positions were derived by using the weighting scheme described in Reference D2 (in its second section, "Coordinate Transformation").

Table D3
STADAN—Optical—Source B.*

Name	Station No.	Latitude	Longitude	Geodetic Height (meters)	Datum
1BPOIN	1021	38°25'49".63 38 25 49.44	282°54'48".23 282 54 48.65	5 -50	N.A. C-5
1FTMYR	1022	26 32 51.89 26 32 53.08	278 08 03.93 278 08 03.80	19 -42	N.A. C-5
1OOMER	1024	-31 23 30.07 -31 23 26.96	136 52 11.05 136 52 14.25	152 148	Australian C-5
1QUITO	1025	-0 37 28.00 -0 37 22.63	281 25 14.81 281 25 15.23	3649 3554	N.A. C-5
1LIMAP	1026	-11 46 44.43 -11 46 37.56	282 50 58.23 282 50 58.86	155 34	N.A. C-5
1SATAG	1028	-33 09 07.66 -33 08 58.76	289 19 51.35 289 19 52.59	922 705	N.A. C-5
1MOJAV	1030	35 19 48.09 35 19 47.57	243 06 02.73 243 05 59.18	905 874	N.A. C-5
1JOBUR	1031	-25 52 58.86 -25 53 02.70	27 42 27.93 27 42 25.41	1530 1546	Arc (Cape) C-5
1NEWFL	1032	47 44 29.74 47 44 28.73	307 16 43.37 307 16 46.67	104 58	N.A. C-5
1COLEG	1033	64 52 19.72 64 52 17.78	212 09 47.17 212 09 37.29	162 139	N.A. C-5
1GFORK	1034	48 01 21.40 48 01 20.81	262 59 21.56 262 59 19.55	253 200	N.A. C-5
1WNKFL	1035	51 26 44.12 51 26 40.67	359 18 14.62 359 18 08.35	62 76	European C-5
1ROSMA	1042	35 12 06.93 35 12 07.03	277 07 41.01 277 07 40.81	914 857	N.A. C-5
1TANAN	1043	-19 00 27.09 -19 00 33.26	47 18 00.46 47 17 58.89	1377 1355	Tananarive C-5

*The coordinates in the above table are identical to the corresponding Minitrack site coordinates if the latter exist, since the STADAN MOTS cameras are co-located with the center of the Minitrack antenna array for calibration purposes.

Table D4
STADAN—R/R—Source B.

Name	Station No.	Latitude	Longitude	Geodetic Height (meters)	Datum
MADGAR	1122	-19°01'13".32 -19 01 19.41	47°18'09".45 47 18 07.96	1403 1382	Tananarive C-5
ROSRAN	1126	35 11 45.05 35 11 45.15	277 07 26.23 277 07 26.02	880 823	N.A. C-5
CARVON	1152	-24 54 14.85 -24 54 12.29	113 42 55.05 113 42 58.54	38 10	Australian C-5

Table D5

Navy TRANET—Doppler—Source C.

Name	Station No.	Latitude	Longitude	Geodetic Height (meters)	Datum
LASHAM	2006	51°11'10".62	358°58'30".51	182	European
		51 11 07.12	358 58 24.25	196	C-5
SANHES	2008	-23 13 01.74	314 07 50.59	608*	Corrego Alegre
		-23 13 01.74	314 07 50.59	608	C-5
PHILIP	2011	14 58 57.79	120 04 25.98	8	Tokyo
		14 59 16.42	120 04 21.61	-70	C-5
SMTHFD	2012	-34 40 31.31	138 39 12.39	39	Australian
		-34 40 28.16	138 39 15.66	31	C-5
MISAWA	2013	40 43 04.63	141 20 04.69	-10	Tokyo
		40 43 14.63	141 19 51.45	38	C-5
ANCHOR	2014	61 17 01.98	210 10 37.46	61	N.A.
		61 16 59.60	210 10 28.60	44	C-5
TAFUNA	2017	-14 19 50.19	189 17 13.96	6*	USGS 1962 ASTRO
		-14 19 50.19	189 17 13.96	6	C-5
THULEG	2018	76 32 18.62	291 13 46.72	43	N.A.
		76 32 20.72	291 13 51.07	-7	C-5
MCMRDO	2019	-77 50 51.00	166 40 25.00	-43	Mercury
		-77 50 50.58	166 40 35.02	-29	C-5
WAHIWA	2100	21 31 26.86	202 00 00.63	380	Old Hawaiian
		21 31 14.95	202 00 09.83	368	C-5
LACRES	2103	32 16 43.75	253 14 48.25	1201	N.A.
		32 16 43.91	253 14 45.34	1162	C-5
LASHM2	2106	51 11 12.32	358 58 30.21	187	European
		51 11 08.82	358 58 23.95	201	C-5
APLMND	2111	39 09 47.83	283 06 11.07	146	N.A.
		39 09 47.59	283 06 11.52	90	C-5
PRETOR	2115	-25 56 46.09	28 20 53.00	1417	European
		-25 56 49.97	28 20 50.67	1595	C-5
SHEMYA	2739	52 43 01.52	174 06 51.43	44	N.A.
		52 42 56.52	174 06 44.17	89	C-5
BELTSV	2742	39 01 39.46	283 10 27.25	50	N.A.
		39 01 39.23	283 10 27.72	-5	C-5
STNVIL	2745	33 25 31.57	269 09 10.70	44	N.A.
		33 25 31.76	269 09 09.66	-10	C-5

*MSL.

Table D6
Air Force—Optical—Source I.*

Source	Name	Station No.	Latitude	Longitude	Geodetic Height (meters)	Datum
	ANTIGA	3106	17°08'51".68	298°12'37".41	7	N.A.
			17 08 53.88	298 12 39.19	-42	C-5
E	GRNVLE	3333	33 28 48.97	268 59 49.17	45	N.A.
			33 28 49.15	268 59 48.12	-9	C-5
	GRVILL	3334	33 25 31.95	269 05 11.35	43	N.A.
			33 25 32.14	269 05 10.30	-10	C-5
	USAFAC	3400	39 00 22.44	255 07 01.01	2191	N.A.
			39 00 21.99	255 06 58.32	2147	C-5
E	BEDFRD	3401	42 27 17.53	288 43 35.03	88	N.A.
			42 27 17.06	288 43 36.14	33	C-5
E	SEMMES	3402	30 46 49.35	271 44 52.37	79	N.A.
			30 46 49.85	271 44 51.64	23	C-5
	SWANIS	3404	17 24 16.57	276 03 29.87	83	N.A.
			17 24 18.90	276 03 29.71	18	C-5
	GRDTRK	3405	21 25 47.05	288 51 14.03	7	N.A.
			21 25 48.69	288 51 15.03	-48	C-5
	CURACO	3406	12 05 22.11	291 09 43.76	23	N.A.
			12 05 25.49	291 09 45.16	-34	C-5
	TRNDAD	3407	10 44 32.78	298 23 23.67	269	N.A.
			10 44 36.16	298 23 25.43	210	C-5
	GRANFK	3451	47 56 38.63	262 37 11.21	296	N.A.
			47 56 38.03	262 37 09.15	242	C-5
	TWINOK	3452	36 07 25.69	262 47 04.48	312	N.A.
			36 07 25.58	262 47 02.68	262	C-5
	ROTHGR	3453	51 25 00.00	9 30 06.00	351	European
			51 24 57.05	9 30 00.58	352	C-5
	ATHNGR	3463	37 53 30.00	23 44 30.00	16	European
			37 53 26.07	23 44 26.73	23	C-5
	TORRSP	3464	40 29 18.53	356 34 41.24	588	European
			40 29 14.10	356 34 36.06	635	C-5
	CHOFUJ	3465	35 39 57.00	139 32 12.00	49	Tokyo
			35 40 08.96	139 32 00.19	75	C-5
	KINDLY	3471	32 22 57.30	295 19 00.46	26	N.A.
			32 22 57.41	295 19 02.09	-23	C-5
E	HUNTER	3648	32 00 05.87	278 50 46.36	17	N.A.
			32 00 06.32	278 50 46.32	-40	C-5
	JUPRAF	3649	27 01 14.80	279 53 13.72	26	N.A.
			27 01 16.02	279 53 13.72	-37	C-5
E	ABERDN	3657	39 28 18.97	283 55 44.56	4	N.A.
			39 28 18.71	283 55 45.10	-51	C-5
E	HOMEST	3861	25 30 24.69	279 36 42.69	18	N.A.
			25 30 26.02	279 36 42.70	-44	C-5
	CHYWYN	3902	41 07 59.20	255 08 02.65	1890	N.A.
			41 07 58.61	255 07 59.94	1845	C-5

*Unless "Source" is specified otherwise.

Table D7

Army Map Service--SECOR--Source H.*

Source	Name	Station No.	Latitude	Longitude	Geodetic Height (meters)	Datum
G	HERNDN	5001	38°59'37.69	282°40'16.68	119	N.A.
			38 59 37.47	282 40 17.08	64	C-5
I	CUBCAL	5200	32 48 00.00	242 52 00.00	101	N.A.
			32 47 59.74	242 51 56.55	71	C-5
I	LARSON	5201	47 11 00.00	240 40 00.00	354	N.A.
			47 10 58.76	240 39 55.68	319	C-5
I	WRGTON	5202	43 39 00.00	264 25 00.00	481	N.A.
			43 38 59.49	264 24 58.27	428	C-5
G	GREENV	5333	33 25 32.34	269 05 10.78	43	N.A.
			33 25 32.53	269 05 09.73	-10	C-5
	TRUKIS	5401	7 27 39.30	151 50 31.28	5 [†]	Navy IBEN ASTRO 1947
			7 27 39.30	151 50 31.28	5	C-5
	SWALLO	5402	-10 18 21.42	166 17 56.79	9 [†]	1966 SECOR ASTRO
			-10 18 21.42	166 17 56.79	9	C-5
	KUSAIE	5403	5 17 44.43	163 01 29.88	7 [†]	ASTRO 1962, 65 Allen Sodano Lt.
			5 17 44.43	163 01 29.88	7	C-5
	GIZZOO	5404	-8 05 40.58	156 49 24.82	49 [†]	Provisional DOS
			-8 05 40.58	156 49 24.82	49	C-5
	TARAWA	5405	1 21 42.13	172 55 47.26	7 [†]	1966 SECOR ASTRO
			1 21 42.13	172 55 47.26	7	C-5
	NANDIS	5406	-17 45 31.01	177 27 02.83	17 [†]	Viti Levu 1916
			-17 45 31.01	177 27 02.83	17	C-5
	CANTON	5407	-2 46 28.99	188 16 43.47	6 [†]	1966 Canton ASTRO
			-2 46 28.99	188 16 43.47	6	C-5
	JONSTN	5408	16 43 51.68	190 28 41.55	6 [†]	Johnston Island 1961
			16 43 51.68	190 28 41.55	6	C-5
	MIDWAY	5410	28 12 32.06	182 37 49.53	6	Midway ASTRO 1961
			28 12 32.06	182 37 49.53	6	C-5
	MAUIHI	5411	20 49 37.00	203 31 52.77	32	Old Hawaiian
			20 49 25.14	203 32 01.88	31	C-5
G	FTWART	5648	31 55 18.41	278 26 00.26	29	N.A.
G	HNTAFB	5649	31 55 18.86	278 26 00.18	-27	C-5
			32 00 04.04	278 50 43.17	27	N.A.
G	HOMEFL	5861	32 00 04.49	278 50 43.13	-30	C-5
			25 29 21.18	279 37 39.35	18	N.A.
			25 29 22.51	279 37 39.37	-44	C-5

*Unless "Source" is specified otherwise.

†MSL.

Table D8

USC&GS—Optical—Source F.

Name	Station No.	Latitude	Longitude	Geodetic Height (meters)	Datum
BELTVL	6002	39°01'39.03	283°10'26.94	45	N.A.
		39 01 38.80	283 10 27.40	-10	C-5
ASTRMD	6100	39 01 39.72	283 10 27.83	45	N.A.
		39 01 39.49	283 10 28.29	-10	C-5
TIMINS	6113	48 33 56.17	278 37 44.54	290	N.A.
		48 33 55.70	278 37 44.49	232	C-5

Table D9

SPEOPT—Optical—Source B.

Name	Station No.	Latitude	Longitude	Geodetic Height (meters)	Datum
1UNDAK	7034	48°01'21.40	262°59'21.56	255	N.A.
		48 01 20.81	262 59 19.55	201	C-5
1EDINB	7036	26 22 45.44	261 40 09.03	67	N.A.
		26 22 46.35	261 40 07.34	15	C-5
1COLBA	7037	38 53 36.07	267 47 42.12	271	N.A.
		38 53 35.81	267 47 40.85	218	C-5
1BERMD	7039	32 21 48.83	295 20 32.56	21	N.A.
		32 21 48.94	295 20 34.18	-28	C-5
1PURIO	7040	18 15 26.22	294 00 22.17	58	N.A.
		18 15 28.30	294 00 23.63	5	C-5
1GSFCP	7043	39 01 15.01	283 10 19.93	54	N.A.
		39 01 14.78	283 10 20.39	-1	C-5
1CKVLE	7044	38 22 12.50	274 21 16.81	187	N.A.
		38 22 12.33	274 21 16.28	131	C-5
1DENVR	7045	39 28 48.03	255 23 41.19	1796	N.A.
		39 38 47.54	255 23 38.52	1751	C-5
1JUM24	7071	27 01 12.77	279 53 12.31	25	N.A.
		27 01 14.00	279 53 12.30	-38	C-5
1JUM40	7072	27 01 13.17	279 53 12.49	25	N.A.
		27 01 14.39	279 53 12.49	-38	C-5
1JUPC1	7073	27 01 13.11	279 53 12.72	22	N.A.
		27 01 14.33	279 53 12.72	-41	C-5
1JUBC4	7074	27 01 13.33	279 53 12.76	25	N.A.
		27 01 14.55	279 53 12.76	-38	C-5
1SUDBR	7075	46 27 20.99	279 03 10.35	281	N.A.
		46 27 20.52	279 03 10.35	224	C-5
1JAMAC	7076	18 04 31.98	283 11 26.52	485	N.A.
		18 04 34.20	283 11 27.03	423	C-5

Table D10
SPEOPT—Laser—Source B.

Name	Station No.	Latitude	Longitude	Geodetic Height (meters)	Datum
GODLAS	7050	39°01'13".68	283°10'18".05	55	N.A.
		39 01 13.45	283 10 18.51	0	C-5
ROSLAS	7051	35 11 46.60	277 07 26.23	879	N.A.
		35 11 46.70	277 07 26.02	822	C-5

Table D11
International—Optical—Source I.*

Source	Name	Station No.	Latitude	Longitude	Geodetic Height (meters)	Datum
D	DELFTH	8009	52°00'09".24	4°22'21".23	23	European
			52 00 06.12	4 22 15.30	28	C-5
	ZIMWLD	8010	46 52 41.77	7 27 57.56	903	BERNE
			46 52 36.73	7 27 52.54	907	C-5
	MALVRN	8011	52 08 39.12	358 01 59.49	111	European
			52 08 35.68	358 01 53.03	125	C-5

*Unless "Source" is specified otherwise.

Table D12
SAO—Optical.

Name	Station No.	Location
1ORGAN	9001	Organ Pass, New Mexico
1OLFAN	9002	Olifantsfontein, South Africa
WOOMER	9003	Woomera, Australia
1SPAIN	9004	San Fernando, Spain
1TOKYO	9005	Tokyo, Japan
1NATOL	9006	Naini Tal, India
1QUIPA	9007	Arequipa, Peru
1SHRAZ	9008	Shiraz, Iran
1CURAC	9009	Curacao, Lesser Antilles
1JUPTR	9010	Jupiter, Florida
1VILDO	9011	Villa Dolores, Argentina
1MAUIO	9012	Maui, Hawaii
OSLONR	9426	Oslo, Norway
AUSBAK	9023	Woomera, Australia
NATALB	9029	Natal, Brazil
AGASSI	9050	Cambridge, Massachusetts
COLDLK	9424	Cold Lake, Alberta
EDWAFB	9425	Edwards AFB, California
RIGLAT	9428	Riga, Latvia
POTDAM	9429	Potsdam, Germany
ZVENIG	9430	Zvenigorod, Russia

Table D13
STADAN—Optical.

Name	Station No.	Location
1BPOIN	1021	Blossom Point, Maryland
1FTMYR	1022	Fort Myers, Florida
1OOMER	1024	Woomera, Australia
1QUITO	1025	Quito, Ecuador
1LIMAP	1026	Lima, Peru
1SATAG	1028	Santiago, Chile
1MOJAV	1030	Mojave, California
1JOBUR	1031	Johannesburg, Union of South Africa
1NEWFL	1032	St. John's, Newfoundland
1COLEG	1033	College, Alaska
1GFORK	1034	East Grand Forks, Minnesota
1WNKFL	1035	Winkfield, England
1ROSM	1042	Rosman, North Carolina
1TANAN	1043	Tananarive, Madagascar

Table D14
STADAN—R/R.

Name	Station No.	Location
MADGAR	1122	Tananarive, Madagascar
ROSRAN	1126	Rosman, North Carolina
CARVON	1152	Carnarvon, Australia

Table D15
Navy TRANET—Doppler.

Name	Station No.	Location
LASHAM	2006	Lasham, England
SANHES	2008	Sao Jose dos Campos, Brazil
PHILIP	2011	San Miquel, Philippines
SMTHFD	2012	Smithfield, Australia
MISAWA	2013	Misawa, Japan
ANCHOR	2014	Anchorage, Alaska
TAFUNA	2017	Tafuna, American Samoa
THULEG	2018	Thule, Greenland
MCMRDO	2019	McMurdo Sound, Antarctica
WAHIWA	2100	South Point, Hawaii
LACRES	2103	Las Cruces, New Mexico
LASHM2	2106	Lasham, England
APLMND	2111	APL Howard County, Maryland
PRETOR	2115	Pretoria, Union of South Africa
SHEMYA	2739	Shemya Island, Alaska
BELTSV	2742	Beltsville, Maryland
STNVIL	2745	Stoneville, Mississippi

Table D16

Air Force—Optical.

Name	Station No.	Location
ANTIGA	3106	Antigua Island, Lesser Antilles
GRNVLE	3333	Stoneville, Mississippi
GRVILL	3334	Stoneville, Mississippi
USAFAC	3400	Colorado Springs, Colorado
BEDFRD	3401	L. G. Hanscom Field, Massachusetts
SEMMES	3402	Semmes Island, Georgia
SWANIS	3404	Swan Island, Caribbean Sea
GRDTRK	3405	Grand Turk, Caicos Islands
CURACO	3406	Curacao, Lesser Antilles
TRNDAD	3407	Trinidad Island
GRANFK	3451	Grand Forks, North Dakota
TWINOK	3452	Twin Oaks, Oklahoma
ROTHGR	3453	Rothwesten, West Germany
ATHNGR	3463	Athens, Greece
TORRSP	3464	Torrejon de Ardoz, Spain
CHOFUJ	3465	Chofu, Japan
KINDLY	3471	Kindley AFB, Bermuda
HUNTER	3648	Hunter AFB, Georgia
JUPRAF	3649	Jupiter, Florida
ABERDN	3657	Aberdeen, Maryland
HOMEST	3861	Homestead AFB, Florida
CHYWYN	3902	Cheyenne, Wyoming

Table D17

Army Map Service—SECOR.

Name	Station No.	Location
HERNDN	5001	Herndon, Virginia
CUBCAL	5200	San Diego, California
LARSON	5201	Moses Lake, Washington
WRGTON	5202	Worthington, Minnesota
GREENV	5333	Greenville, Mississippi
TRUKIS	5401	Truk Island, Caroline Islands
SWALLO	5402	Swallow Island, Santa Cruz Islands
KUSAIE	5403	Kusaie Island, Caroline Islands
GIZZOO	5404	Gizzoo, Gonzongo, Solomon Islands
TARAWA	5405	Tarawa, Gilbert Islands
NANDIS	5406	Nandi, Viti Levu, Fiji Islands
CANTON	5407	Canton Island, Phoenix Islands
JONSTN	5408	Johnston Island, Pacific Ocean
MIDWAY	5410	Eastern Island, Midway Islands
MAUIHI	5411	Maui, Hawaii
FTWART	5648	Fort Stewart, Georgia
HNTAFB	5649	Hunter AFB, Georgia
HOMEFL	5861	Homestead AFB, Florida

Table D18

USC&GS—Optical.

Name	Station No.	Location
BELTVL	6002	Beltsville, Maryland
ASTRMD	6100	Beltsville, Maryland
TIMINS	6113	Timmins, Ontario

Table D19

SPEOPT—Optical.

Name	Station No.	Location
1UNDAK	7034	Univ. North Dakota, Grand Forks, North Dakota
1EDINB	7036	Edinburg, Texas
1COLBA	7037	Columbia, Missouri
1BERMD	7039	Bermuda Island
1PURIO	7040	San Juan, Puerto Rico
1GSFCP	7043	GSFC, Greenbelt, Maryland
1CKVLE	7044	Clarksville, Indiana
1DENVR	7045	Denver, Colorado
1JUM24	7071	Jupiter, Florida
1JUM40	7072	Jupiter, Florida
1JUPC1	7073	Jupiter, Florida
1JUBC4	7074	Jupiter, Florida
1SUDBR	7075	Sudbury, Ontario
1JAMAC	7076	Jamaica, B. W. I.

Table D20

SPEOPT—Laser.

Name	Station No.	Location
GODLAS	7050	GSFC, Greenbelt, Maryland
ROSLAS	7051	Rosman, North Carolina

Table D21

International—Optical.

Name	Station No.	Location
DELFTH	8009	Delft, Holland
ZIMWLD	8010	Berne, Switzerland
MALVRN	8011	Malvern, England

REFERENCES

1. Lundquist, C. A., and Veis, G., "Geodetic Parameters for a 1966 Smithsonian Institution Standard Earth," Smithsonian Astrophysical Observatory Special Report No. 200, Vol. 1, 1966.
2. Lerch, F. J., Marsh, J. G., D'Aria, M. D., and Brooks, R. L., "GEOS I Tracking Station Positions on the SAO Standard Earth (C-5)," NASA Technical Note D-5034, August 1968.
3. Lerch, F. J., Doll, C. E., Moss, S. J., and O'Neill, B., "The Determination and Comparison of the GRARR MADGAR Site Location," NASA Technical Note D-5033, August 1968.

Appendix E

**Table of GEOS 1 Orbit Numbers from
12/31/65 to 1/5/66**



Table E1

Pass Numbers for GEOS I.
(Mean Period of GEOS I at epoch 12/31/65 $01^{\text{H}} 38^{\text{M}} 22^{\text{S}} = 2^{\text{H}}005393 = 120^{\text{M}}3236$)

Pass No.	From			To		
650	12/31/65	01 ^H	18 ^M	12/31/65	03 ^H	17 ^M
651		03	18		05	17
652		05	18		07	18
653		07	19		09	18
654		09	19		11	18
655		11	19		13	18
656		13	19		15	19
657		15	20		17	19
658		17	20		19	19
659		19	20		21	20
660		21	21		23	20
661		23	21	01/01/66	01	20
662	01/01/66	01	21		03	21
663		03	22		05	21
664		05	22		07	21
665		07	22		09	21
666		09	22		11	22
667		11	23		13	22
668		13	23		15	22
669		15	23		17	23
670		17	24		19	23
671		19	24		21	23
672		21	24		23	24
673		23	25	01/02/66	01	24
674	01/02/66	01	25		03	24
675		03	25		05	24
676		05	25		07	25
677		07	26		09	25
678		09	26		11	26
679		11	26		13	26
680		13	27		15	26
681		15	27		17	26
682		17	27		19	27
683		19	28		21	27
684		21	28		23	27
685		23	28	01/03/66	01	28
686	01/03/66	01	29		03	28
687		03	29		05	28
688		05	29		07	28
689		07	29		09	29
690		09	30		11	29
691		11	30		13	29
692		13	30		15	30
693		15	31		17	30
694		17	31		19	30
695		19	31		21	31
696		21	32		23	31
697		23	32	01/04/66	01	31

Table E1—Continued

Pass No.	From			To			
698	01/04/66	01 ^H	32 ^M	01/04/66	03 ^H	31 ^M	
699		03	32		05	32	
700		05	33		07	32	
701		07	33		09	32	
702		09	33		11	33	
703		11	34		13	33	
704		13	34		15	33	
705		15	34		17	34	
706		17	35		19	34	
707		19	35		21	34	
708		21	35		23	34	
709		23	35		01/05/66	01	35
710		01/05/66	01			36	03
711	03		36	05		35	
712	05		36	07		36	

FIRST CLASS MAIL



POSTAGE AND FEES PAID
NATIONAL AERONAUTICS AND
SPACE ADMINISTRATION

070 001 32 51 305 70033 00903
AIR FORCE WEAPONS LABORATORY / WL01 /
KIRTLAND AFB NEW MEXICO 87117

THE NATIONAL COLLECTION LIBRARY

POSTMASTER: If Undeliverable (Section 151
Postal Manual) Do Not Return

"The aeronautical and space activities of the United States shall be conducted so as to contribute . . . to the expansion of human knowledge of phenomena in the atmosphere and space. The Administration shall provide for the widest practicable and appropriate dissemination of information concerning its activities and the results thereof."

— NATIONAL AERONAUTICS AND SPACE ACT OF 1958

NASA SCIENTIFIC AND TECHNICAL PUBLICATIONS

TECHNICAL REPORTS: Scientific and technical information considered important, complete, and a lasting contribution to existing knowledge.

TECHNICAL NOTES: Information less broad in scope but nevertheless of importance as a contribution to existing knowledge.

TECHNICAL MEMORANDUMS: Information receiving limited distribution because of preliminary data, security classification, or other reasons.

CONTRACTOR REPORTS: Scientific and technical information generated under a NASA contract or grant and considered an important contribution to existing knowledge.

TECHNICAL TRANSLATIONS: Information published in a foreign language considered to merit NASA distribution in English.

SPECIAL PUBLICATIONS: Information derived from or of value to NASA activities. Publications include conference proceedings, monographs, data compilations, handbooks, sourcebooks, and special bibliographies.

TECHNOLOGY UTILIZATION PUBLICATIONS: Information on technology used by NASA that may be of particular interest in commercial and other non-aerospace applications. Publications include Tech Briefs, Technology Utilization Reports and Notes, and Technology Surveys.

Details on the availability of these publications may be obtained from:

**SCIENTIFIC AND TECHNICAL INFORMATION DIVISION
NATIONAL AERONAUTICS AND SPACE ADMINISTRATION
Washington, D.C. 20546**